ARCHIVES OF CIVIL ENGINEERING, LVI, 1, 2010

DOI: 10.2478/v.10169-010-0002-0

FINITE ELEMENT MODELLING OF THE BEHAVIOUR OF A CERTAIN CLASS OF COMPOSITE STEEL-CONCRETE BEAM-TO-COLUMN JOINTS

M. A. GIŻEJOWSKI[1], W. BARCEWICZ[2], W. SALAH[3]

Beam-to-column end-plate joints can be classified as rigid (fully restrained), semi-rigid (partially restrained) or pinned, depending on their type, configuration and the connector arrangement. Fully restrained joints are needed for rigid frames in which there is assumed that the frame joints have sufficient rigidity to maintain – under the service state – the angles between the intersecting members, ensuring the full moment transfer. In contrast in semi-continuous frames, partially restrained joints are characterized by relative rotations occurring between the intersecting members so that the bending moment can only be transferred partially. In recent years, the idea of using partially restrained, unstiffened joints in building structures has gained momentum since this idea appears to be more practical and economical. Semi-continuous frames can resist actions by the bending moment transfer in partially restrained joints, allowing in the same time for a certain degree of rotation that enhances the overall ductile performance of these structures. One of the effective ways that affects ductility of end-plate beam-to-column joints is to use thinner end-plates than those used nowadays in practical applications. In the current study, a certain class of steel-concrete composite joints is examined in which the thickness of end-plates is to be equivalent to approximately 40-60% of the bolt diameter used in all the composite joints investigated in the considered joint class. This paper is an extension of the authors' earlier investigation on numerical modelling of the behaviour of steel frame joints. The aim of current investigations is to develop as simple as possible and yet reliable three-dimensional (3D) FE model of the composite joint behaviour that is capable of capturing the important factors controlling the performance of steel-concrete end-plate joints in which the end-plate thickness is chosen to be lesser than that used nowadays in conventional joint detailing. A 3D FE model constructed for composite joints of the considered joint class is reported in this paper and numerical simulations using the ABAQUS computer code are validated against experimental investigations conducted at the Warsaw University of Technology. Comparison between the nonlinear FE analysis and full scale experimental results of the considered class of composite joints is presented which conclusively allows for the accuracy assessment of the modelling technique developed. Comparison between the FE results and test data shows a reasonable agreement between the numerical FE model developed and physical model of experimentally examined joint specimens. Finally, practical conclusions for engineering applications are drawn.

[1] PhD. DSc., Faculty of Civil Engineering, Warsaw University of Technology, Poland, e-mail: m.gizejowski@il.pw.edu.pl

[2] PhD Student, Faculty of Civil Engineering, Warsaw University of Technology, Poland, e-mail: w.barcewicz@il.pw.edu.pl

[3] PhD, Civil Engineering Department, Al-Azhar University, Cairo, Egypt, e-mail: waelcivil@hotmail.com; formerly PhD Student, Faculty of Civil Engineering, Warsaw University of Technology, Poland

Key words: joint, composite, steel-concrete, end-plate, finite element model, nonlinear analysis, inelastic behaviour.

1. INTRODUCTION

Composite structures, exploring advantages of concrete and structural steel, have been increasingly applied in commercial and parking buildings. The effective application of steel and concrete leads to the increased strength and stiffness if compared with traditional solutions such as bare steel or reinforced concrete structural elements. Due to advantages of composite construction, the scope of application of composite actions in steel frameworks have been widened, finally involving not only the composite action between the structural floor beams and the reinforced concrete slab, but also taking advantage of composite joints. Design rules for composite joints were developed on the basis of worldwide research efforts since there had been rather limited guidance and lack of expertise in this field, e.g. SIMÕES DA SILVA *et al.* [1]. Existing design rules of Eurocode 4 [2] are not however general since they do not cover all possible solutions, especially in design of composite joints.

Investigations into understanding of the beam-to-column joint behaviour have commenced at the beginning of the last century, see BRÓDKA and KOZLOWSKI [3], among others. Originally, most of the studies were dedicated to steel structures and focused on estimation of the load carrying capacity and prediction of the structural behaviour in terms of load–deflection curves and failure mechanisms. Recent steelwork Eurocode 3 [4] includes the practical aspects of the steel joint behaviour prediction in terms of stiffness, strength and rotation capacity. More recently, research has been directed towards the behaviour of composite joints (refer to KOZLOWSKI [5], BRÓDKA and KOZLOWSKI [6]). The nonlinear analysis of composite structures, carried out up to the failure limit, is rather difficult due to the complexity of physical phenomena accompanying the structure deterioration process under increasing actions, bond interaction between concrete and steel parts, stress redistribution between the concrete and steel reinforcement after cracking, interaction of the behaviour of steel beam shear studs and concrete, the presence of any profiled metal decking, occurrence of slip between the steel parts and reinforced concrete slab, and due to a variety of all other possible local effects existing in the structure composed of such different materials like steel and concrete, with regard to the overall ductility behaviour. Modelling of composite steel-concrete end-plate joints can be conveniently carried out after the detailed investigations of the bare steel end-plate joint behaviour and full understanding of the composite steel-concrete beam behaviour. The results for end-plate joints are greatly influenced by the behaviour of end-plates and bolts. In end-plate beam-to-column joints where the thickness of the end-plate is smaller than that used nowadays in steel frame systems, the bolt failure is purposefully prevented and the joint behaviour is to be controlled by the ductility of end-plate and their weld connectors, see GIŻEJOWSKI *at al.* [7] – for flush end-plates

and [8] – extended end-plates. Results of these investigations are considered herein together with modelling techniques developed for composite beams.

Composite steel-concrete beams are formed typically from rolled sections and reinforced concrete slab of a constant thickness or a variable thickness when slab is cast in-situ on profiled sheeting, see JOHNSON [9], UY and LIEW [10], KUCHARCZUK and LABOCHA [11]. In case of profiled sheeting used for in-situ casting, it is treated as a lost decking or it is assumed to play the role of an additional reinforcement of the composite beam subjected to service loads. During the past two decades, different FE software packages were used to study the nonlinear behaviour of composite structures. OVEN *et al.* [12] developed a two dimensional nonlinear FE model for the analysis of composite beams with partial interaction. This model is based on a plane frame nonlinear finite element analysis implemented to the computer code program INSTAF, originally developed for steel frames. A numerical model that allows for a reliable analysis of the composite steel-concrete beams was proposed by FABBROCINO *et al.* [13]. This proposed model was able to describe the main mechanical phenomenon of the composite beams under sagging bending. In addition, a generalized relationship of the moment-curvature characteristic was proposed. BASKAR and SHANMUGAM [14] developed 3D FE model using ABAQUS code to analyse four simply supported composite plate girders. The flanges, web and stiffener plates of the steel girder were modelled by 8-node doubly curved thin shell elements and the concrete deck slab by thick shell elements. Reinforcement was modelled with the REBAR LAYER option available in the ABAQUS code. LIANG *et al.* [15] developed a 3D FE model to consider the geometric and material nonlinear behaviour of continuous composite beams. The FE program ABAQUS was utilized to investigate the strength of continuous composite beams under the combined effects of bending and shear. The four-node doubly curved general shell elements with reduced integration were employed to model the concrete slab, the flanges and the web of the steel beam. The stud shear connectors were modelled using 3D beam elements. Huber-von-Mises yield criterion was employed in the nonlinear analysis treating the material plasticity with five integration points through the element thickness. BASKAR *et al.* [16] carried out a numerical study using the ABAQUS code to predict the ultimate behaviour of composite steel-concrete beams under negative moment and shear loading. Various combinations of material models and finite element types were investigated to identify a suitable modelling technique for prediction of the ultimate load behaviour of composite plate girders. Web, flanges and stiffeners were idealized using the element S8R5 that is the 8-node doubly curved thin shell element, with reduced integration points, using five degrees of freedom (DOFs) per node. The steel-concrete interaction was modelled by two different approaches: (1) surface interaction technique, and (2) modelling with 3D beam elements. Concrete slab was modelled with the finite element C3D20 that is the 20-node quadratic brick element, and reinforcing bars were represented with using an ABAQUS option of REBAR LAYER. Bond strength at the steel-concrete interface and shear studs were combined and modelled as horizontal friction shear between the two interaction surfaces. 3D refined FE modelling technique

for simply supported composite beams using the ABAQUS code was described in detail by Barth and Wu [17]. A four-node general purpose shell elements S4R with reduced integration were used to model the steel girder, concrete slab and stiffeners. The steel reinforcement in concrete was modelled by means of REBAR LAYER that is an available option in ABAQUS enabling to account for the effect of reinforced concrete. Full composite action between the concrete slab and the top flange of the steel girder was considered using beam type multi-point constraints (MPCs). Chung and Sotelino [18] investigated element compatibility and geometric error for the 3D FE modelling technique of composite steel-concrete girder bridges. Five 3D composite bridge models were analyzed using the general purpose FE software package ABAQUS. Queiroz *et al.* [19] conducted a numerical study on simply supported composite beams considering the full and partial shear connection using ANSYS software. The shell element SHELL43 defined by four nodes and having six DOFs at each node was used to model the steel section. The used shell element allowed for plasticity, creep, stress stiffening, large deformation and large strain capability. The solid element SOLID65 with eight nodes and three translation DOFs at each node was assigned to represent the concrete slab. The nonlinear spring element COMBIN39, defined by two-node points, was adopted to simulate the shear connectors. Both longitudinal and transversal reinforcing bars were modelled as smeared throughout the solid elements. Fu *el al.* [20] used the continuum elements available in the ABAQUS code to model semi-rigid composite joints with precast hollow core slabs. 3D continuum elements were used to model all parts of the composite joints and the contact was applied explicitly between all the joint components. Gizejowski *et al.* [21] developed a modelling technique using the ABAQUS code and spring elements to represent the contribution of the shear stud behaviour to account for the different degree of composite action. Gizejowski and Salah [22] discussed various aspects of this modelling technique for the discretized composite beams, and used the outcomes from a number of simulations for an adequate modelling of composite beams. Numerical simulations were carried out to model the composite joint with the use of different element types. The authors pointed out some crucial modelling parameters that can significantly influence the modelling of composite joints, such as mesh size of the concrete slab, type of the element to be used for modelling of the steel-concrete interaction and parameters affecting the constitutive model of concrete.

This paper presents an initial study for modelling of composite steel-concrete beam-to-column joints. The class of joints considered is based on their steel counterparts that were tested and numerically modelled by the authors in the earlier studies [7, 8]. Design of these joints varies widely, so that it is impossible to develop a general analytical model for the prediction of joint response. Instead, beam-to-column joint tests were conducted in order to determine the relationship describing the way in which the moment is transferred through the joint components. Practical behavioural joint models usually include a limited number of parameters taken into account from test data. Thus, there is a need to numerically generate a reliable moment-rotation response

of semi-rigid composite joints that can be used for calibration of an analytical expression for the spring moment-rotation characteristic applied in engineering practice for analysis and design, refer to GIŻEJOWSKI *et al.* [23]. The FE analysis conducted herein employs the ABAQUS code (see ABAQUS manuals [24], [25]) in order to precisely simulate the various configurations of tested composite joints. The configuration of composite joints is the same as for bare steel flush end-plate beam-to-column joints analyzed by the authors in [7] and for bare steel extended end-plate joints analyzed in [8]. The only difference is that composite joints are additionally equipped with the concrete slab cast on the steel decking made of profiled sheeting and with steel shear stud connectors ensuring the composite action between the reinforced concrete slab and the steel rolled I-section beam.

2. BRIEF DESCIPTION OF EXPERIMENTAL INVESTIGATIONS USED FOR VALIDATION OF FE MODELLING TECHNIQUE

Within the current research project, conducted in the Department of Building Structures of the Warsaw University of Technology, laboratory tests were designed in order to investigate the behaviour of steel and steel-concrete composite joints under bending conditions. The results of eight tests on composite beam-to-column joints are reported. The steelwork part of the connection uses an end-plate welded to the beam and bolted to the column flange. The influence of detailing of end-plate connections with respect to thickness and height of the end-plate and also a number and position of the bolts, depending on the height of the end-plate, as well as the influence of different reinforcement ratio of the slab, is described. Two types of end-plates are used in the tests: flush and extended. Applied end-plates were relatively thin, i.e. the thickness of about 40-60% of the bolt diameter used in the end-plate-to-column-flange connection. For the purpose of comparing, the bare steel specimens were also tested with the same arrangement as the steelwork part of composite steel-concrete joints. The general arrangement of composite joint specimens is presented in Fig. 1. The joints detailing is given in Table 1.

Beam elements of all the specimens were made of IPE 300 and the columns of HEB 200. All the steel elements (beams, columns and end-plates) were made of steel grade S235JR. The bolt connectors were M20 of class 10.9. The concrete slab was cast on the dip-profiled sheeting, using the Cofraplus 60 composite flooring. The ribs of the sheeting were arranged in the transverse direction to the supporting beams. The composite action was partially provided by the sheeting and the headed studs (SD ϕ19 $\times$ 100 mm) that were friction welded to the upper flange of the beam. The concrete class was of C25/30 (B30). The main slab reinforcing bars were made of steel grade BSt500S. Tested composite specimens were divided into two groups, depending on the reinforcement ratio. An amount of the reinforcing bars was constant in both groups. The only difference was the diameter of the bars. In the first series, the diameter

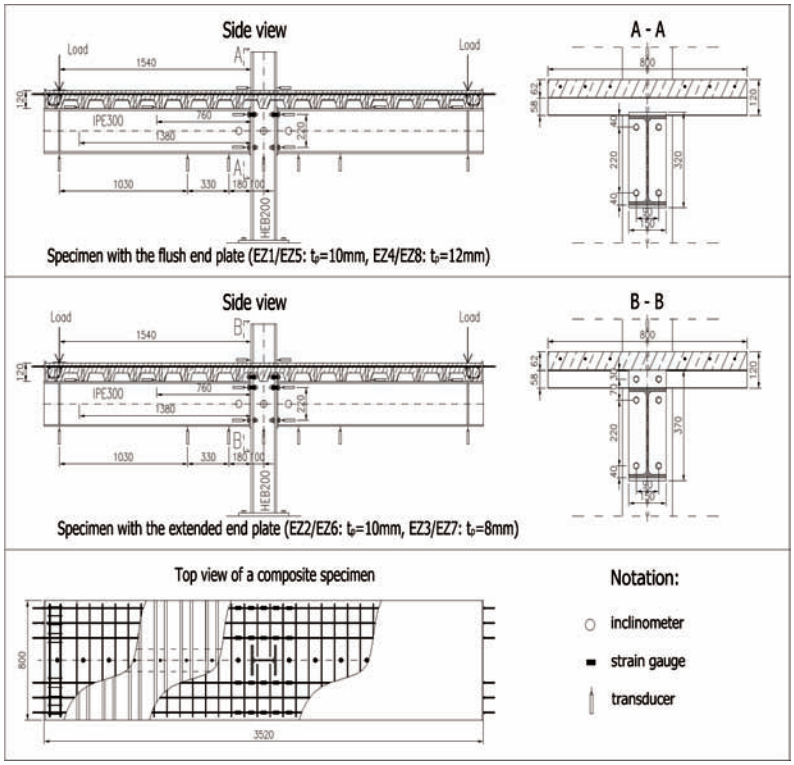

Fig. 1. Summary of tested specimens.
Rys. 1. Zestawienie elementów próbnych

was 8 mm, giving the reinforcement ratio of about 0.60% and in the second one – 12 mm, giving this ratio of about 1.35% with respect to the total depth of the slab above the ribs. The effective width of the slab of 800 mm was used. The transverse reinforcement consisted of bars of the diameter 6 mm. Under the position of load application, additional embedded beam-like strips reinforced with 4 bars of 12 mm in diameter were designed to prevent concrete crushing on edges of the slab.

All the tests were conducted for the static loading increasing monotonically till failure. Two independent jacks were used to apply the same loads on each cantilever tip, at 1540 mm from the column face. The symmetrical arrangement was used to control the specimen behaviour and any effect of imperfections that can cause the column drift. A general view of setup of the test rig is shown in Fig. 2. The testing procedure and the load history were designed using the moment resistance of joint specimens calculated according to the component method of Eurocodes EN 1993-1-8 [4] and EN 1994-1-1 [2].

The measurements taken for bare steel specimens were described in details in [7]. The same positions and techniques of recording the measured readings were adopted

Table 1

Summary of tested specimens.
Zestawienie elementów próbnych

Specimen groups (concrete slab reinforcing bars)	End-plate thickness t_p (mm)	Symbol used for joint	Type of end-plate
Group #0 Bare steel joints	10	ES1	Flush
	12	ES4	
	10	ES2	Extended
	8	ES3	
Group #1 Composite joints (6 ϕ 8 mm)	10	EZ1	Flush
	12	EZ4	
	10	EZ2	Extended
	8	EZ3	
Group #2 Composite joints (6 ϕ 12 mm)	10	EZ5	Flush
	12	EZ8	
	10	EZ6	Extended
	8	EZ7	

in case of all the composite specimens tested. Moreover, for composite specimens additional measurements were taken such as: deflection of the column by means of inductive transducers positioned outside of the column flanges, above the slab; strains in the longitudinal reinforcement bars by strain gauges; slip between the slab and beam by means of inductive transducers located on the top surface of the beam flange near the ribs of the slab at two points of each cantilever; strains in the concrete slab by the adaptive gauge and crack width by a microscope. An arrangement of the instrumentation for tested specimens is shown in Fig. 1 as well as in Fig. 2.

By comparing the experimental results of the composite joints and those obtained for the corresponding bare steel joints, one could conclude that adding the concrete slab to the bare steel joint enhances the performance of such a joint in terms of both the initial stiffness and the ultimate moment. Regarding the increase of the initial stiffness, there are factors of 2.1 for EZ1 and 2.5 for EZ5, indicating the ratio of the stiffness of composite joints to the stiffness of their steel counterpart ES1, the joint with flush end-plate of 10 mm in thickness. For the composite joints with the flush end-plate of 12 mm in thickness, namely EZ4 and EZ8, the initial stiffness increased by factors 1.7 and 2.2, respectively, if compared with the stiffness of bare steel specimen ES4. The higher value of stiffness belongs to the group with the higher reinforcement ratio. There is a similar situation when the joint ultimate moment is taken into account. For specimens with the rebars of 8 mm in diameter, the ratio of the specimen EZ1 ultimate moment to that of specimen ES1 is equal to 1.7 and for the specimens EZ4 compared to ES4 this factor is equal to 1.6. For the specimens with the reinforcement of 12 mm in diameter, the ratio of the specimen EZ5 ultimate moment to that of specimen ES1 is equal to 2.3 and for the specimens EZ8 compared to ES4 this factor is equal to 2.2.

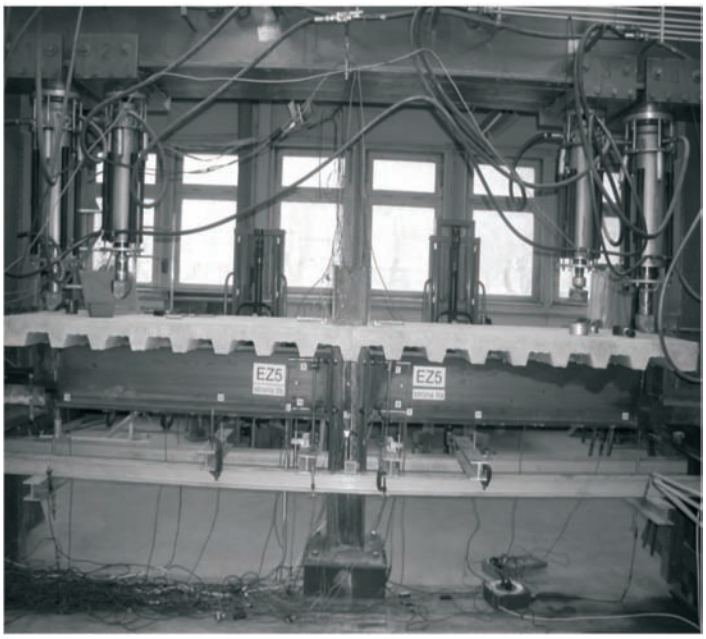

Fig. 2. General setup of the test rig.
Rys. 2. Widok ogólny stanowiska badawczego

The results for the bare steel joint with extended end-plate proved that the existence of the concrete slab had a positive influence on the joint initial stiffness and the ultimate moment capacity. The ratios depicting the increase of the initial stiffness for each composite joint with extended end-plate in relation to its bare steel counterpart are following: for the group of specimens with the lower diameter of reinforcing bars (8 mm) – 1.5 for specimen EZ2 in relation to ES2, 1.4 for specimen EZ3 in relation to ES3, and for the group with the bigger diameter (12 mm) of the rebars – 1.8 for specimen EZ6 in relation to ES2, 1.7 for specimen EZ7 in relation to ES3. The similar comparisons are made for the evaluation of the increase of the ultimate moment and they are presented below: for the first group 1.3 for specimen EZ2 with reference to ES2, 1.4 for specimen EZ3 with reference to ES3 and for the second group 1.5 for specimen EZ6 with reference to ES2, 1.8 for specimen EZ7 with reference to ES3. These increased values of the initial stiffness as well as the ultimate moment of composite joints if compared with their steel counterparts proved that taking into account a composite action of the joint results in visible economical profits.

The only disadvantage of the composite joints behaviour is a lower ductility at the ultimate strength if compared with that observed for their steel counterparts (without the concrete slab, decking and shear connectors).

As to the assessment of the mode of failure, the experimental investigations proved that the brittle fracture of reinforcement is achieved at the ultimate strength for joints

with the lower reinforcement ratio while for the joint with a higher value of this ratio – the ductile mode governed that was associated with the excessive yielding of the column web panel, regardless the end-plate form (flush or extended) and the plate thickness.

3. DESCRIPTION OF FINITE ELEMENT MODELLING TECHNIQUE DEVELOPED

As it has been stated in the introduction, FE models developed and numerical simulations performed for the purpose of this paper are based on the FE package ABAQUS. The 3D refined FE modelling technique is used to investigate numerically the behaviour of composite steel-concrete beam-to-column joints tested experimentally. Nonlinearity resulting from the behaviour of materials employed for composite joint components and geometric nonlinearity are considered for all the load-displacement FE simulations. A general 3D view of modelled steel-concrete composite joints is depicted in Fig. 3. All the modelling details of steel beam-to-column joint components are the same as considered in the shell FE modelling technique described by the authors in [7, 8].

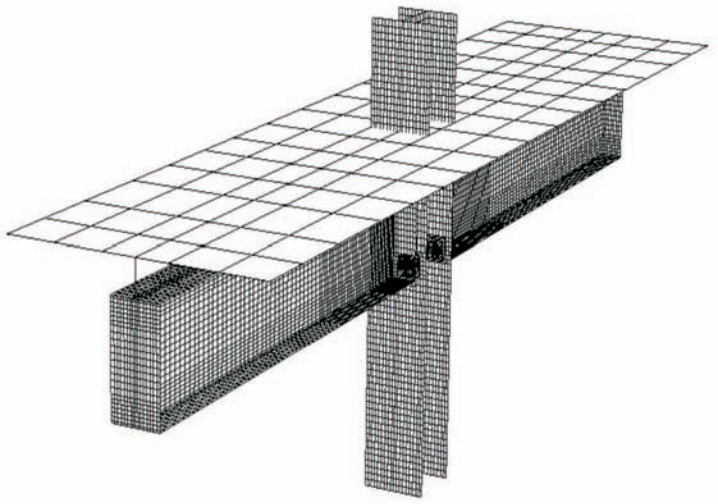

Fig. 3. 3D FE mesh for one of the analyzed composite joints.
Rys. 3. Przestrzenna siatka elementów skończonych przykładowego węzła zespolonego

3.1. MODELLING OF CONCRETE

In the hogging moment regions, the concrete slab is mainly under tension. Modelling of concrete in negative bending regions is more complex than that in sagging zones since subjected to tension. Since the concrete is weak in tension, it behaves in a

softening manner after reaching a certain strain value at the low level of load application. In FE analysis, Smeared Crack (SC) model available in ABAQUS is used to model the concrete material. In the SC model, cracking is assumed to occur when the stress reaches a failure surface that is called "the crack detection surface". This failure surface represents a linear relationship between the equivalent pressure stress, p, and the Huber-von-Mises equivalent deviatoric stress, q. When a crack has been detected, its orientation is stored for the subsequent calculations. Further cracking at the same point is restricted to being orthogonal to this direction since the stress components in concrete with an open crack are not included in the direction of the failure surface used for the detection of additional cracks.

The CONCRETE option available in ABAQUS is used to define the stress-strain behaviour of plain concrete not only in uniaxal tension but also in uniaxial compression outside the elastic range. Idealized concrete stress-strain relationship is diagrammatically shown in Fig. 4. In tension it is considered that concrete is a linear elastic material up to the uniaxial tensile strength, and then a certain degradation model, e.g. the linear model as shown in Fig. 4, has to represent the concrete post-limit behaviour in tension. The post-limit behaviour for direct straining across cracks is modelled with a TENSION STIFFENING option in ABAQUS. This option allows for modelling of the behaviour of cracked reinforced concrete, since it allows for the bonding effects and shear interaction between the reinforcing bars and concrete.

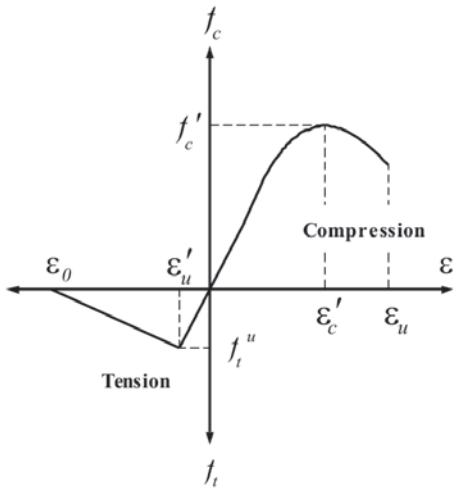

Fig. 4. Idealized uniaxial stress-strain relationship for concrete.
Rys. 4. Idealizowana zaleznosc naprezenie-odksztalcenie dla betonu

Average values of the strength and stiffness properties of concrete obtained from material tests for concrete of composite joints investigated experimentally are given in

Table 2. The zero stress post-limit tensile strain factor used in the numerical simulations is taken as 0.1.

Table 2

Average values of concrete properties.
Uśrednione wartości właściwości betonu

Specimen groups	Concrete class	E (MPa)	f_c'(MPa)	$\varepsilon_u^{*)}$	f_t^u (MPa)	$\varepsilon_0^{*)}$
Group #1	C25/30	36515	45.7	0.003	3.2	0.1
Group #2	C25/30	36314	50.5	0.003	3.6	0.1
*) Recommended default values						

Concrete slab is modelled using thick 4-node general shell elements S4. Only the top flat part of the concrete slab with thickness of 62 mm (see Fig. 1) is considered in FE analysis and the shell elements representing the concrete slab are placed in the middle thickness of the concrete flat part. The scheme with coarse mesh size of approximately ten times the steel parts mesh size – as suggested by GIŻEJOWSKI and SALAH [22] – is used to discretize the concrete slab.

3.2. MODELLING OF REINFORCEMENT

The steel reinforcement in the concrete slab is provided by means of REBAR LAYER that is an available option in ABAQUS for modelling of reinforcing bars in the reinforced concrete section. As it is described before, only the top flat part of the concrete slab is modelled and the effect of the concrete ribs is ignored for modelling simplicity. As a result, the actual reinforcement ratio referred to a concrete constant thickness of the concrete slab section of tested specimens is considered in numerical simulations.

The classical bilinear steel plasticity model of an elastic-plastic type with strain hardening is used for the inelastic material effects occurring in the reinforcement. This idealized stress-strain curve is shown in Fig. 5 and used hereafter to represent the material nonlinearity in the REBAR LAYER.

Average numerical values of steel reinforcement properties evaluated from material tests for joint specimens tested in the laboratory are given in Table 3.

Table 3

Average values of steel reinforcement properties used for concrete slab.
Uśrednione wartości właściwości stali zbrojeniowej płyty stropowej

Diameter	Steel grade	E*) (MPa)	f_y (MPa)	f_u (MPa)	ε_u
8	BSt500S	200000	668.9	751.2	0.175
12	BSt500S		638.1	728.9	0.177
*) Characteristic value used					

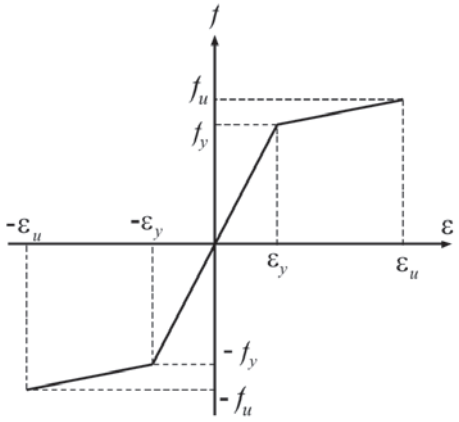

Fig. 5. Idealized bilinear stress-strain relationship for steel reinforcing bars and shear connectors.
Rys. 5. Idealizowana dwuliniowa zależność naprężenie-odkształcenie dla prętów zbrojenia i łączników zespalających

3.3. Modelling of shear connectors

Beam element type B31, based on Timoshenko beam theory allowing for shear strain deformations, is used to model the stud shear connectors. A circular cross section is used for studs. The idealized stress-stain relationship presented in Fig. 5 is used to model not only the reinforcement but also to represent the material nonlinearity of the shear stud connectors.

Average numerical values of stud properties evaluated from material tests for joint specimens are given in Table 4.

Table 4

Average values of shear stud steel properties.
Uśrednione wartości właściwości stali łączników zespalających

Diameter x height	Steel grade	E*) (MPa)	f_y (MPa)	f_u (MPa)	ε_u
19 x 100	S235J2G3+C450	210000	502	537	0.19
*) Characteristic value used					

3.4. Modelling of structural steel components

Thin four-node shell elements with reduced integration and with five DOFs per node S4R5 are used to model all components of the steel beam, column and end-plate. Classical trilinear plasticity models of elastic-plastic type with strain hardening are used for the nonlinear material effects occurring in all the components of beams, columns and end-plates. This idealized stress-strain curve is shown in Fig. 6 and used hereafter to represent the material nonlinearity for the finite elements of structural

steel components. Bolt material is modelled with use of the bilinear characteristic as for reinforcing bars of the concrete slab (see subsection 3.2).

Average numerical values of structural steel and bolt properties, evaluated from material tests for joint specimens tested in the laboratory are given in Table 5.

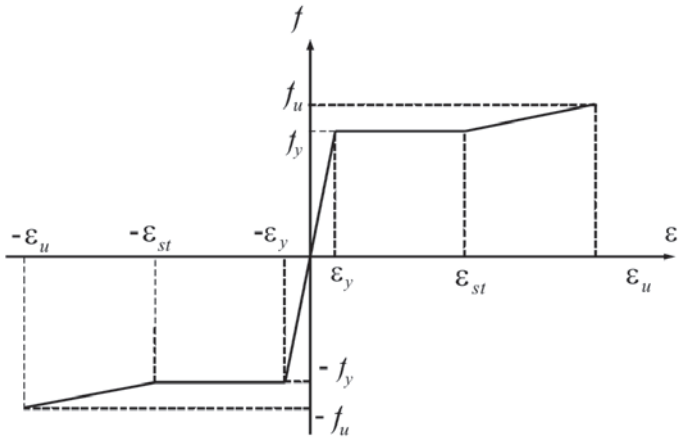

Fig. 6. Idealized trilinear stress-strain relationship for steel structural components.
Rys. 6. Idealizowana trójliniowa zależność naprężenie-odkształcenie dla stali konstrukcyjnej

Table 5

Average values of steel properties for the structural steel used for joint components.
Uśrednione wartości właściwości stali konstrukcyjnej składników węzła

Specimen component	Steel grade	E*) (MPa)	f_y (MPa)	f_u (MPa)	ε_{st}	ε_u
Column section HEB	S235JR	210000	300.6	424.1	0.014	0.372
Beam section IPE	S235JR		321.3	434.9	0.015	0.333
End-plates 12 mm	S235JR		352.1	465.8	0.017	0.205
End-plates 10 mm	S235JR		318.0	454.4	0.015	0.307
End-plates 8 mm	S235JR		284.7	397.6	0.014	0.392
Bolts*)	10.9		940	1040	–	0.09
*) Characteristic values used						

4. RESULTS OF FINITE ELEMENT MODELLING AND VALIDATION OF FE TECHNIQUE USED

The main aim of this study is to trace numerically the behaviour of bolted beam-to--column composite joints with various end-plate thicknesses, different size of end-plates and various ratios of concrete slab reinforcement. According to what has previously been described, eight composite specimens belonging to two groups were tested up

to failure. The former is related to four specimens with the slab reinforcing bars of 8 mm in the diameter while the latter – to four specimens with the same number of reinforcing bars but with the diameter of 12 mm. Eight FE models are therefore created, four for each group, to simulate the tested composite joints with use of the ABAQUS code. The incrementally increased loads were applied to the tested specimens through two hydraulic jacks. They are represented in the numerical analysis via vertical displacements at the free beam ends that are increasing incrementally and proportionally in time to a single parameter. The Modified Riks analysis is adopted for all the numerical simulations.

The results of the FE analysis are presented in terms of load-deflection curves corresponding to the end-beam displacement and the applied load, and in terms of the characteristics corresponding to the joint rotation and the bending moment. Results of the FE analysis are compared to those obtained experimentally. Because of the symmetrical arrangement of the tested specimens and generally similar responses of joints on each side of the specimen column, the curves obtained experimentally come from the average values of measurements recorded for the joints placed on both sides of the column.

Moreover, the results of the bare steel beam-to-column joints presented by the authors in [7, 8] are recalled also hereafter in order to compare them with these of composite joints. The aim of such a comparison is to predict the increase in stiffness and strength of steel joints when their performance is enhanced by adding the concrete slab cast in situ on profiled sheeting formwork, and when ensuring its composite action through shear studs welded to steel beams. It is proven by experiments that composite beam-to-column joints are stronger from their steel counterparts even though the added concrete slab is cracked when exposed to tension due to the negative bending moment.

4.1. Flush end-plate joints

Figures 7-14 show comparison between the test data and the FE results for flush beam-to-column joints. Figure 7 shows the end beam load-displacement curves for the specimens EZ1 and ES1 while the joint M-ϕ curves are presented in Fig. 8. The conducted comparison indicates that the FE model is able to predict with high accuracy of both the initial stiffness and the ultimate moment of the tested composite joint (difference between the ultimate moment results of the FE analysis and the laboratory tests does not exceed 10% for EZ1). The test observations indicated that the failure of the tested specimen EZ1 was reached by developing fracture in the concrete reinforcing bars. The FE analysis is not able to detect such failure since the reinforcement bars are defined in the FE model not as individually discretized structural elements but through the ABAQUS REBAR LAYER option in which the reinforcement is treated as a property in the concrete material. Thus the FE analysis goes beyond the experimentally obtained ultimate load. Numerical analysis can trace the load-deflection behaviour even in the range of large displacements. This range of specimen deformations could not

have been reached in the experimental investigations since the laboratory setup was load controlled and the results could be recorded only up to the ultimate load. Attainment of the ultimate state was recognized as the end of reliable data obtained from the test.

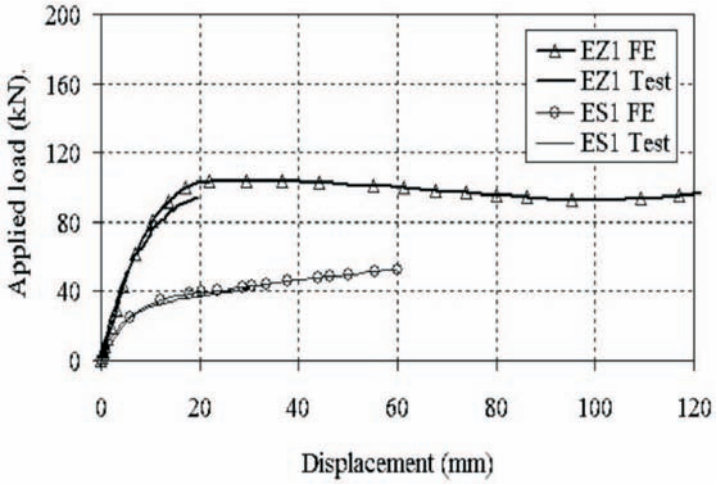

Fig. 7. Load-displacement curves for ES1 and EZ1 specimens; flush end-plate of 10 mm in thickness.
Rys. 7. Krzywe siła-przemieszczenie dla elementów próbnych ES1 i EZ1; blacha zlicowana, t_p=10 mm

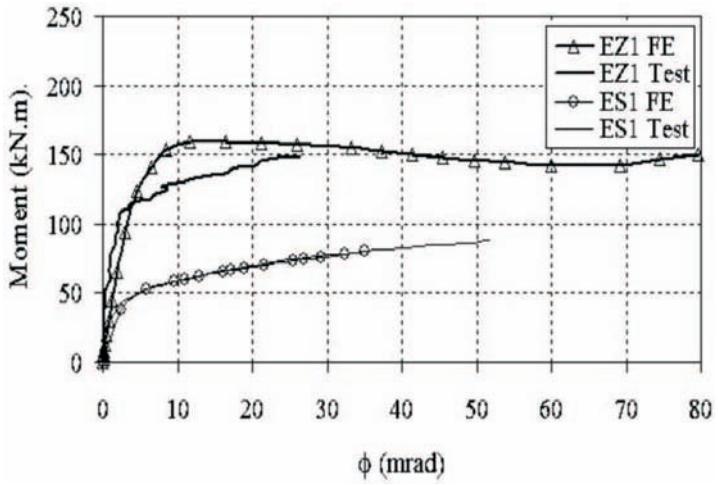

Fig. 8. Moment-rotation curves for ES1 and EZ1 specimens; flush end-plate of 10 mm in thickness.
Rys. 8. Krzywe moment-obrót dla elementów próbnych ES1 i EZ1; blacha zlicowana, t_p=10 mm

The same situation is visible in Fig. 9 and Fig. 10, where load – displacement curves and M-ϕ joint characteristics are presented for specimen EZ4 – the second flush end-plate joint from the group with the smaller reinforcement ratio. Comparison of the

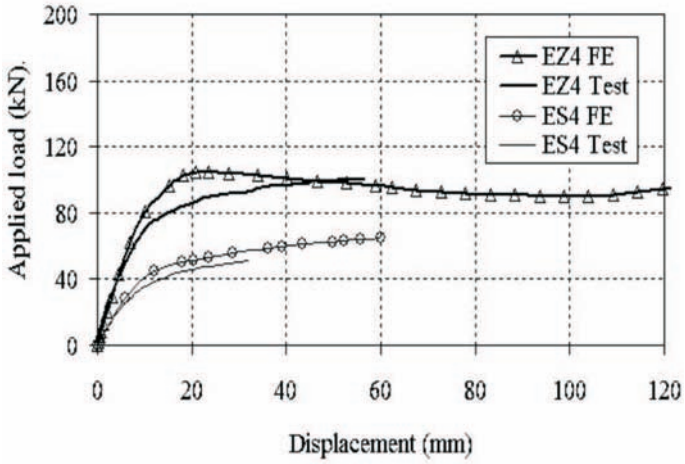

Fig. 9. Load-displacement curves for ES4 and EZ4 specimens; flush end-plate of 12 mm in thickness.
Rys. 9. Krzywe siła-przemieszczenie dla elementów próbnych ES4 i EZ4; blacha zlicowana, t_p=12 mm

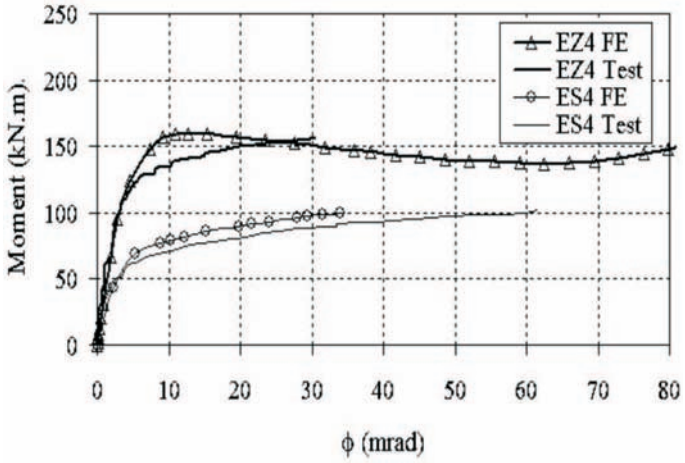

Fig. 10. Moment-rotation curves for ES4 and EZ4 specimens; flush end-plate of 12 mm in thickness.
Rys. 10. Krzywe moment-obrót dla elementów próbnych ES4 i EZ4; blacha zlicowana, t_p=12 mm

maximum value of applied load and the ultimate moment obtained from the tests and FE models, indicates that they are almost the same (the difference between the ultimate moments does not exceed 2%). The only discrepancy is that these ultimate values are reached at a different angle of the joint rotation for the M-ϕ curve and at a different displacement for the load-displacement curve. The ultimate moment for EZ4 FE model is achieved at a smaller value of the joint rotation than that for the steel joint ES4.

Comparing the shapes of the M-ϕ curves for the flush end-plate joints from the first group of composite specimens, namely EZ1 (Fig. 8) and EZ4 (Fig. 10), one can conclude that the best fitting of FE results and test data is noticeable in the elastic range of up to approximately 70% of the ultimate moment. Then a drop in stiffness of the

joints tested experimentally is visible. Beyond that point, the joint stiffness obtained from experimental M-ϕ curves tends to degrade monotonically up to the joint ultimate strength. In curves obtained numerically, a lesser degradation effect is observed, and curves obtained for both specimens are placed above the experimental ones. In M-ϕ curves obtained numerically, a peak point of these curves is reached but it is not related to the failure mode observed in the laboratory tests, namely rupture of reinforcing bars. After reaching the pick point, each of these FE curves descends and finally approaches or crosses the moment capacity level corresponding to that from the laboratory testing.

The comparison of the results obtained for the second group of the composite specimens, consisting of flush end-plate joints EZ5 and EZ8, indicates a certain difference in the shape of FE curves. The failure mode of this group of specimens was related to excessive deformations and local plastic instability of the column web of composite joints, see curves presented in Fig. 11 and Fig. 12 for the specimen EZ5, and in Fig. 13 and Fig. 14 for the specimen EZ8. Shape of the FE and experimental curves, representing the specimen load – displacement characteristics (Fig. 11 and Fig. 13) and the joint moment – rotation characteristics (Fig. 12 and Fig. 14) are closely placed to each other for both types of joint arrangements. It is noticeable not only in the elastic range but also beyond the elastic range, up to the ultimate moment obtained from the FE analysis. Beyond the elastic range, the curves representing the equilibrium path acquired experimentally increase monotonically up to their limit points. Moreover, the experimental ultimate moments associated with limit points are very close to those obtained from the computer simulations (the differences do not exceed 3% for EZ5 and 0% for EZ8). When the FE curves reach their peak value, they start to decrease whereas the experimental ultimate values have to be regarded as the end of test. This results from the limitations of experimental setup which could produce only the force controlled loading history process.

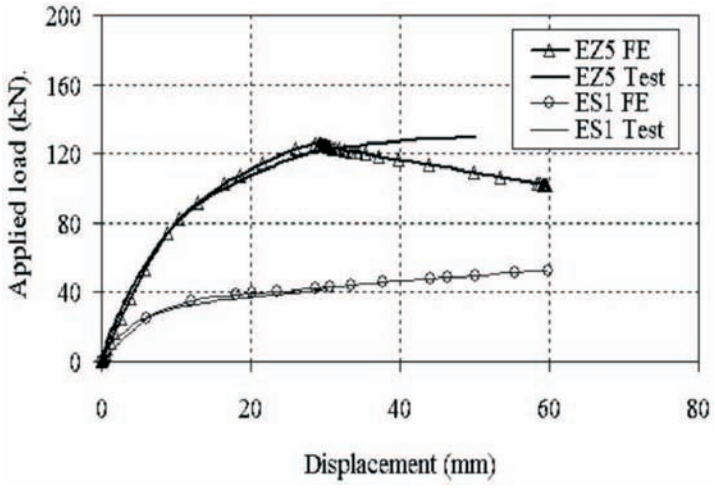

Fig. 11. Load-displacement curves for ES1 and EZ5 specimens; flush end-plate of 10 mm in thickness.
Rys. 11. Krzywe siła-przemieszczenie dla elementów próbnych ES1 i EZ5; blacha zlicowana, t_p=10 mm

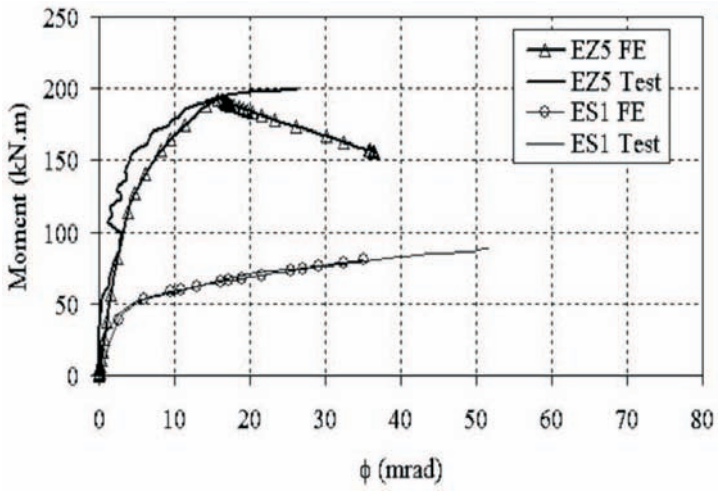

Fig. 12. Moment-rotation curves for ES1 and EZ5 specimens; flush end-plate of 10 mm in thickness.
Rys. 12. Krzywe moment-obrót dla elementów próbnych ES1 i EZ5; blacha zlicowana, t_p=10 mm

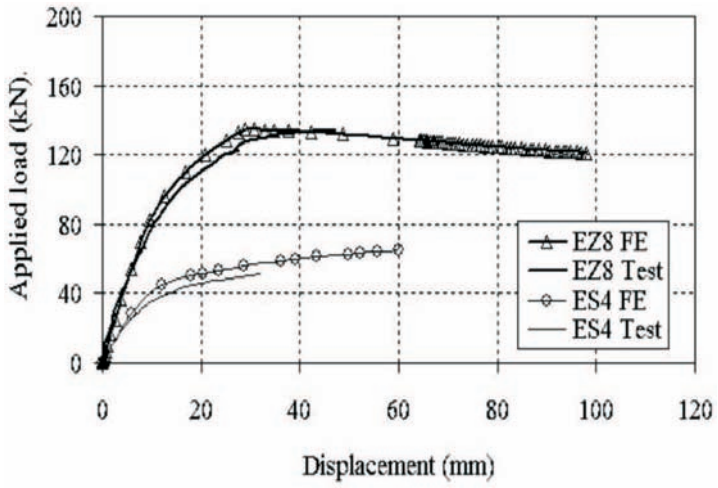

Fig. 13. Load-displacement curves for ES4 and EZ8 specimens; flush end-plate of 12 mm in thickness.
Rys. 13. Krzywe siła-przemieszczenie dla elementów próbnych ES4 i EZ8; blacha zlicowana, t_p=12 mm

4.2. EXTENDED END-PLATE JOINTS

The load-displacement and moment-rotation curves predicted numerically and those resulted from laboratory tests, for all the composite joints with extended end-plates, are shown in Figs. 15-22. The comparison of the load-displacement characteristics

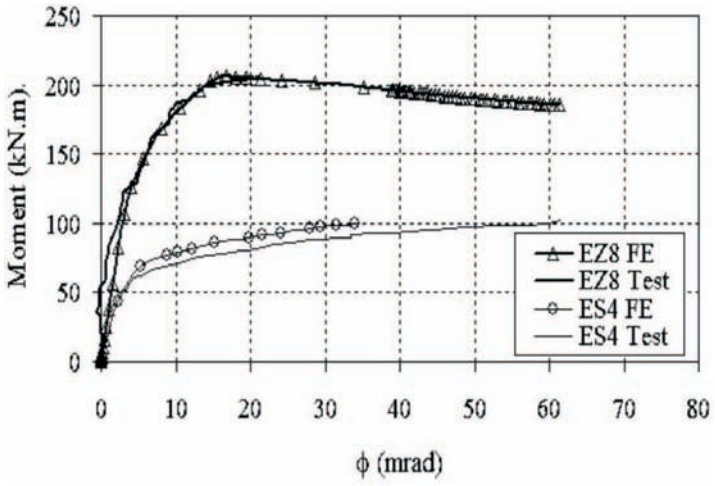

Fig. 14. Moment-rotation curves for ES4 and EZ8 specimens; flush end-plate of 12 mm in thickness.
Rys. 14. Krzywe moment-obrót dla elementów próbnych ES4 i EZ8; blacha zlicowana, t_p=12 mm

obtained for composite joints with extended end-plates, namely EZ3, EZ2, EZ7 and EZ6, are shown in Figs. 15, 17, 19 and 21 while the similar comparison of M-ϕ curves for the same joints is shown in Figs. 16, 18, 20 and 22. With regard to the joint ultimate load, the specimens were examined first separately in two groups, namely the first group of specimens EZ2 and EZ3 with a lower reinforcement ratio, and the second group – specimens EZ6 and EZ7 with a higher reinforcement ratio (see Table 1).

Analysing the first group of specimens (Figs. 15-18), it is noticeable that curves obtained from the FE model are progressing beyond those from experiments. As it has been already mentioned for comparisons made for flush end-plate joints, the loading programme was force controlled, thus the capturing of the post-limit range of the specimen behaviour was not possible in the laboratory testing. Moreover, the actual failure mode observed to occur in the laboratory tests at the limit point of the equilibrium path, resulting from a rapture of reinforcement, could not be reproduced in numerical analysis because of the simplified assumptions associated with the ABAQUS REBAR LAYER option used, as it has been explained previously. It precludes the evaluation of the joint rotational capacity, but it does not hinder one to discuss the main joint properties associated with the joint characteristic, like the ultimate moment and initial stiffness. Comparing the shape of the curves obtained from the tests with the ones from the FE data, one can indicate that the best fitting of these curves is visible in the elastic range. So, the initial stiffness of the specimen EZ2 and EZ3 is modelled properly. Beyond the elastic range, it is noticeable that in the experimental curves there is a faster degradation of the stiffness than that observed for the FE curves. The FE analysis predicts a higher value of the ultimate load and the ultimate moment if compared with that obtained experimentally for composite joints with the low rein-

forcement ratio as it can be observed in Figs. 15-18. For the purpose of comparison with test data, the values assumed to be the numerical ultimate moments are taken at the same level of the joint rotation as that corresponding to the experimental values of ultimate moments. The difference between these values does not however exceed 16% for specimen EZ2 and 23% for specimen EZ3. Moreover, the FE curves run almost parallel to the experimental curves in the plastic range.

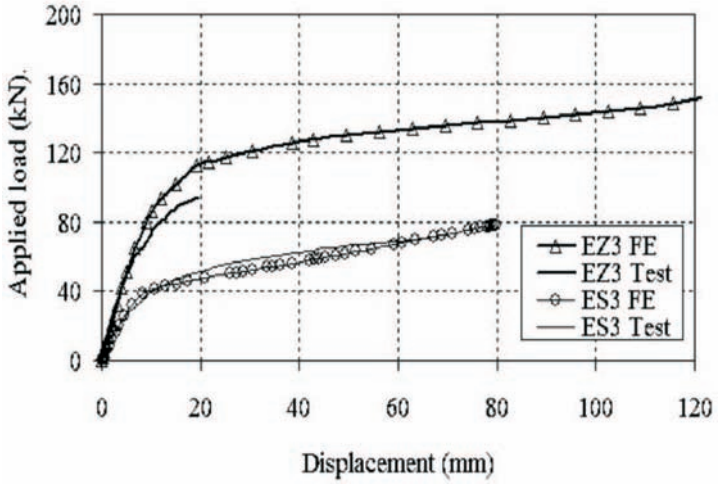

Fig. 15. Load-displacement curves for ES3 and EZ3 specimens; extended end-plate of 8 mm in thickness.
Rys. 15. Krzywe siła-przemieszczenie dla elementów próbnych ES3 i EZ3; blacha wystająca, t_p=8 mm

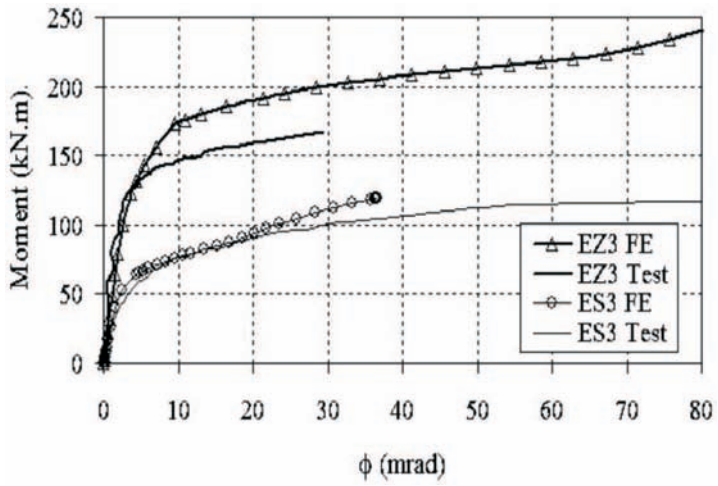

Fig. 16. Moment-rotation curves for ES3 and EZ3 specimens; extended end-plate of 8 mm in thickness.
Rys. 16. Krzywe moment-obrót dla elementów próbnych ES3 i EZ3; blacha wystajaca, t_p=8 mm

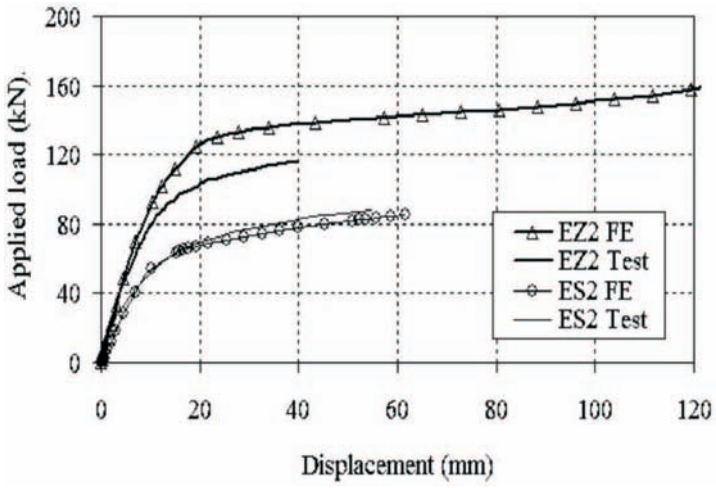

Fig. 17. Load-displacement curves for ES2 and EZ2 specimens; extended end-plate of 10 mm in thickness.
Rys. 17. Krzywe siła-przemieszczenie dla elementów próbnych ES2 i EZ2; blacha wystajaca, t_p=10 mm

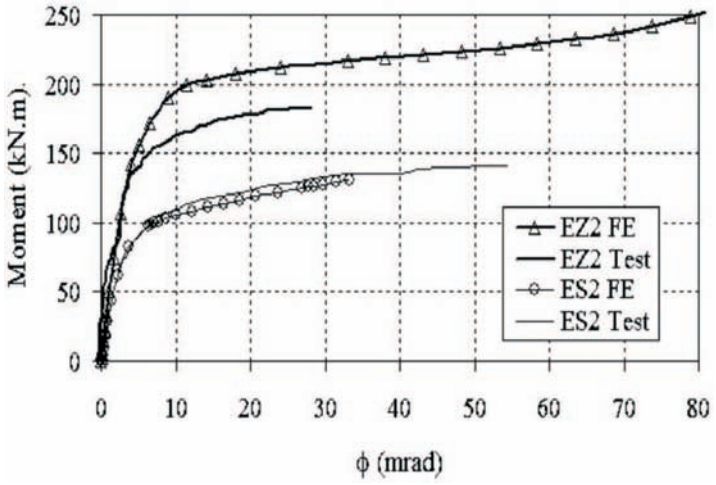

Fig. 18. Moment-rotation curves for ES2 and EZ2 specimens; extended end-plate of 10 mm in thickness.
Rys. 18. Krzywe moment-obrót dla elementów próbnych ES2 i EZ2; blacha wystajaca, t_p=10 mm

On the other hand, the ultimate load obtained numerically is very close to that obtained experimentally for composite joints with the high reinforcement as depicted in Figs. 19-22. This refers not only to the values of ultimate moment but also to the overall behaviour of the considered joints EZ6 and EZ7. The maximum difference between the FE results comparing to the experimental ultimate moment is 6% for EZ6 and -3% for EZ7. Based on the differences between the behaviour simulated with use of FE models and observed for their experimental counterparts for two groups of specimens with extended end-plate joints, one can conclude that the created FE model is more suitable for the group with higher reinforcement ratio, where yielding of the joint compression zone is the governing mode of failure, instead of the rupture of reinforcing bars.

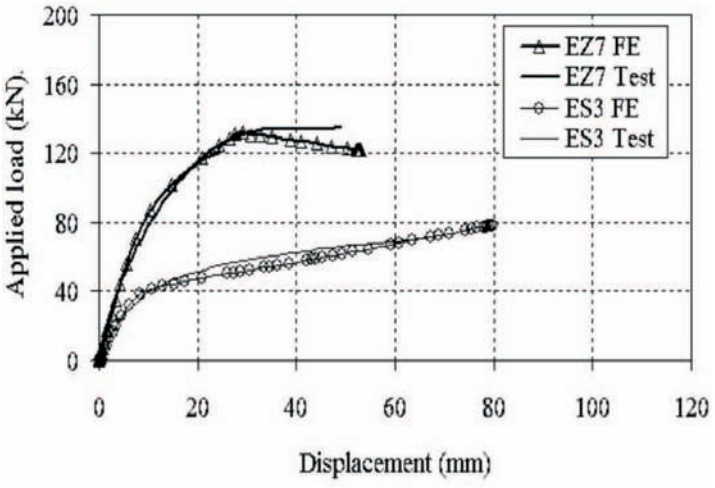

Fig. 19. Load-displacement curves for ES3 and EZ7 specimens; extended end-plate of 8 mm in thickness.
Rys. 19. Krzywe siła-przemieszczenie dla elementów próbnych ES3 i EZ7; blacha wystająca, t_p=8 mm

4.3. Discussion of comparative FE analyses

Many parameters can affect significantly the global behaviour of steel-concrete composite beam-to-column end-plate joints such as the end-plate size, its thickness, the concrete slab reinforcement ratio and the arrangement of shear studs. To investigate the effects of such parameters on the composite joint behaviour, some essential comparisons are carried out in this section. These comparisons are conducted concerning only the M-ϕ relationship for each joint type since this relationship represents the main predictor of the structural frame behaviour.

The first conducted comparison concerns the effect of the end-plate type and its thickness on the behaviour of composite joints. For the same ratio of concrete reinforcement but the different type of end-plates, namely flush and extended, and

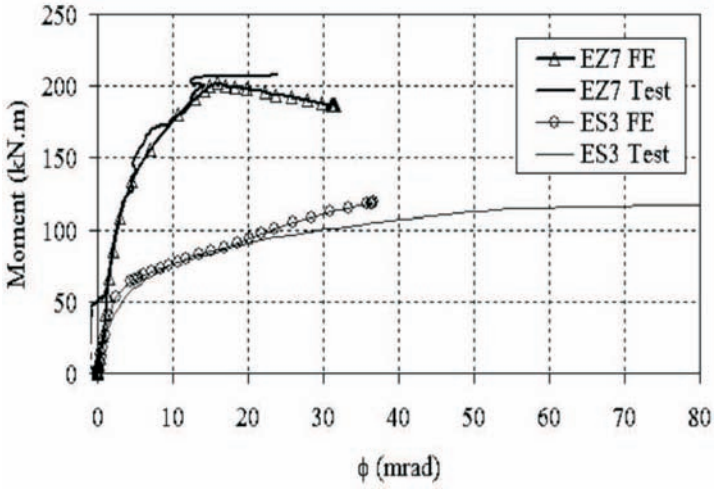

Fig. 20. Moment-rotation curves for ES3 and EZ7 specimens; extended end-plate of 8 mm in thickness.
Rys. 20. Krzywe moment-obrót dla elementów próbnych ES3 i EZ7; blacha wystająca, t_p=8 mm

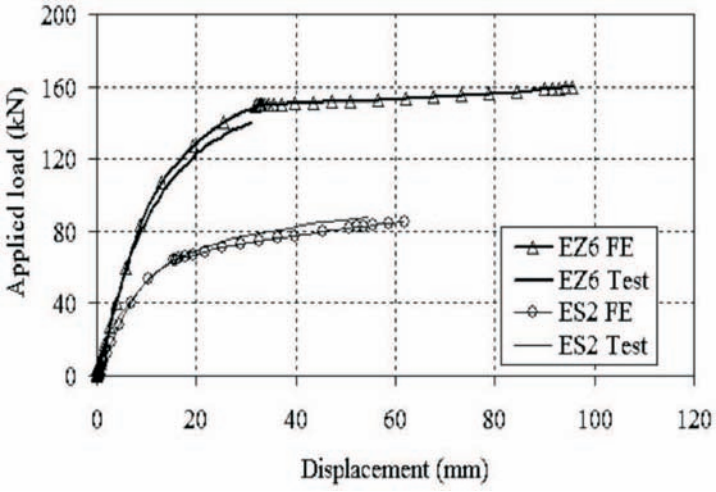

Fig. 21. Load-displacement curves for ES2 and EZ6 specimens; extended end-plate of 10 mm in thickness.
Rys. 21. Krzywe siła-przemieszczenie dla elementów próbnych ES2 i EZ6; blacha wystająca, t_p=10 mm

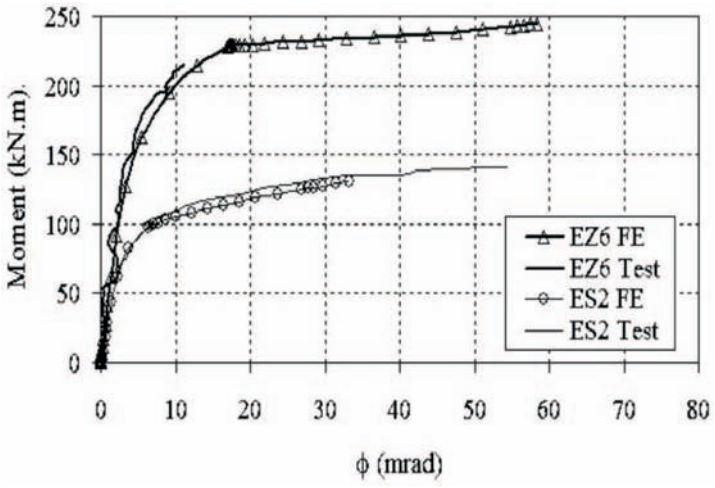

Fig. 22. Moment-rotation curves for ES2 and EZ6 specimens; extended end-plate of 10 mm in thickness.
Rys. 22. Krzywe moment-obrót dla elementów próbnych ES2 i EZ6; blacha wystajaca, t_p=10 mm

the different end-plate thicknesses, namely 8 mm, 10 mm and 12 mm, their M-ϕ characteristics are compared. The FE results obtained for the specimens EZ1 and EZ4, representing flush end-plate joints with the thickness of 10 mm and 12 mm, respectively, and the specimens EZ3 and EZ2, representing extended end-plate joints with the thickness of 8 mm and 10 mm, respectively, are compared in Fig. 23. This comparison indicates that for the same type of end-plates, the end-plate thickness changing within the range of 40%-60% of the bolt diameter has no great influence on the behaviour of the composite joint. On the other hand, extended end-plate joints have a higher moment capacity if compared with that of flush end-plate joints. Also what can be seen from this comparison is that all the composite joints of a different type of the end-plate and a different end-plate thickness ranging from 40% to 60% of the bolt diameter have practically the same initial stiffness. It can be concluded that the presence of concrete is the major factor responsible for the increase of initial stiffness if compared with bare steel joints and the height of end-plate has a noticeable effect on the moment capacity of a certain joint type.

For the second group of specimens used in experiments, the diameter of the concrete reinforcing bars is increased from 8 mm to 12 mm. FE results for specimens EZ5, EZ6, EZ7 and EZ8, i.e. the joints with a relatively high reinforcement ratio, are presented in Fig. 24. Almost the same initial stiffness is observed for the four specimens with different end-plate types and thicknesses. The differences between the ultimate moments obtained numerically are smaller in this case than for specimens with the lower reinforcement ratio. In both groups, however, composite joints with the extended end-plate of 10 mm in thickness, EZ2 and EZ6, have the highest values if compared with all the other specimens included in this comparison exercise.

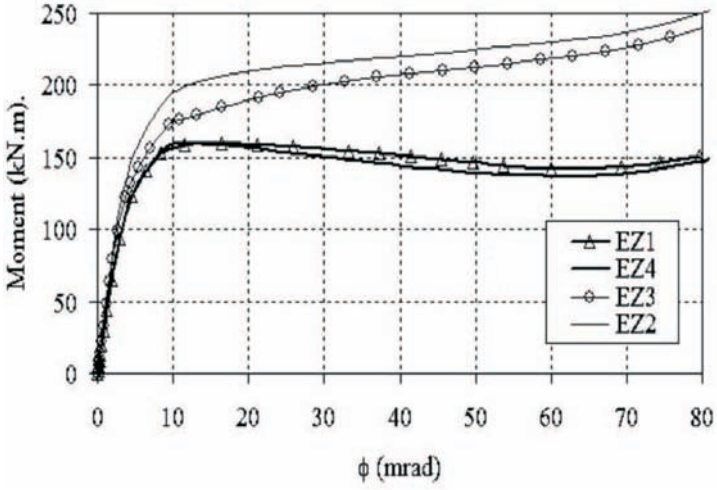

Fig. 23. Moment-rotation curves from numerical FE simulations for various composite joint configurations and different end-pate thicknesses; slab reinforcing bars 6 ϕ 8.
Rys. 23. Krzywe moment-obrót otrzymane z symulacji numerycznej różnych konfiguracji węzłów zespolonych ze względu na grubość i rodzaj blachy czołowej; zbrojenie płyty stropowej 6 ϕ 8

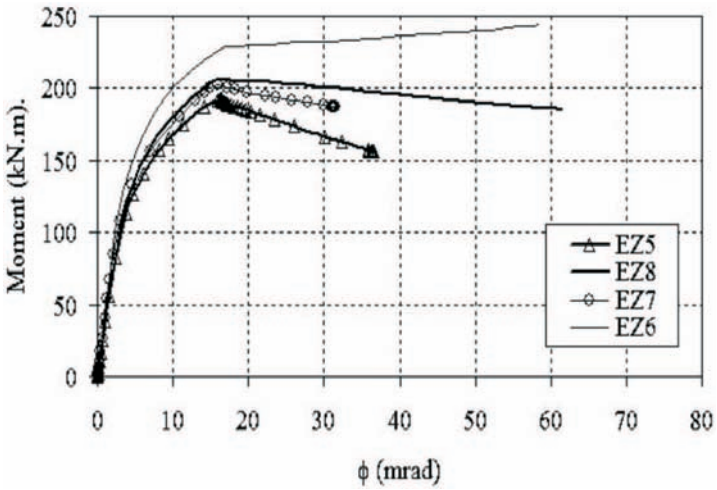

Fig. 24. Moment-rotation curves from numerical FE simulations for various composite joint configurations and different end-pate thicknesses; slab reinforcing bars 6 ϕ 12.
Rys. 24. Krzywe moment-obrót otrzymane z symulacji numerycznej różnych konfiguracji węzłów zespolonych ze względu na grubość i rodzaj blachy czołowej; zbrojenie płyty stropowej 6 ϕ 12

In order to investigate the effect of reinforcement ratio on the behaviour of composite joints, two other comparisons are conducted. In the first comparison, the results for joints with the same type of end-plate are compared with respect to different values of the reinforcement ratio. Figure 25 shows M-ϕ curves for composite joints with the flush end-plate while Fig. 26 presents the FE results for joints with the extended end-plate. Based on these two figures, one can conclude that by adding more reinforcement to the concrete slab, the joint initial stiffness is not significantly affected in case of all the analyzed joints. When the diameter of reinforcing bars is increased but the number of reinforcing bars kept constant, a higher joint moment capacity may be achieved. At the same time, the lesser value of rotation is associated with attainment of the ultimate strength of joints with a higher reinforcement ratio, and this rotation is generally dependent on the amount of reinforcement used.

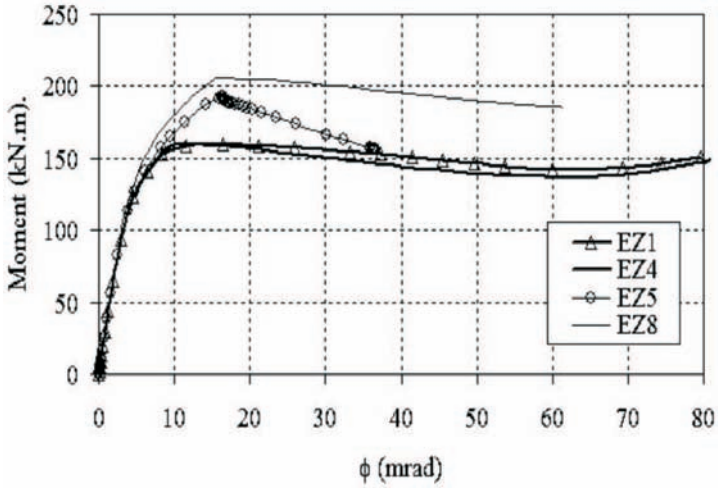

Fig. 25. Moment-rotation curves from numerical FE simulations for flush end-plate composite joints of different end-plate thicknesses and different slab reinforcement ratios.
Rys. 25. Krzywe moment-obrót otrzymane z symulacji numerycznej węzłów zespolonych z blachami czołowymi zlicowanymi, różnicowanych ze względu na grubość blachy i stopień zbrojenia

4.4. Evaluation of stress redistribution process and failure mechanisms

One of the focuses of this study is to investigate the distribution of stresses through the components of tested joints. A precise mapping of the stress distribution is not an easy task in the laboratory therefore the FE analysis is employed herein to capture the stress distribution for all the tested beam-to-column joints. In order to distinguish between the stresses distribution for different arrangements of composite beam-to-column joints, the maps of Huber-von-Mises stresses for all the analyzed joints are captured at an angle of rotation equal to 0.03 radians. Figures 27 and 28 picture the stress distribution for

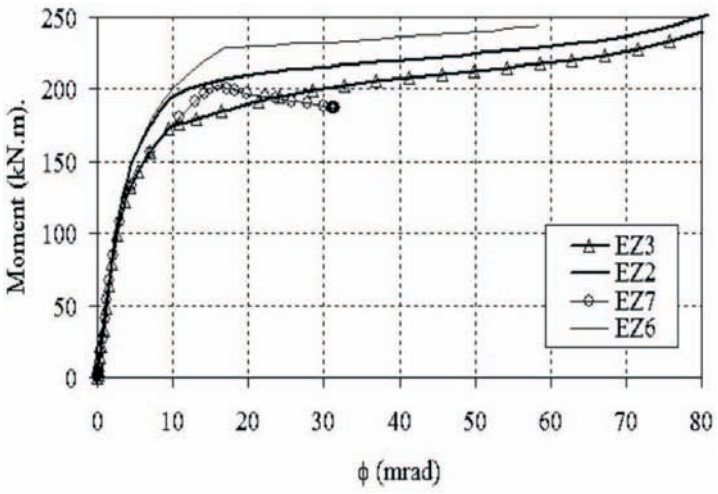

Fig. 26. Moment-rotation curves from numerical FE simulations for extended end-plate composite joints of different end-plate thicknesses and different slab reinforcement ratios.
Rys. 26. Krzywe moment-obrót otrzymane z symulacji numerycznej węzłów zespolonych z blachami czołowymi wystającymi, różnicowanych ze względu na grubość blachy i stopień zbrojenia

twelve tested joints. In case of composite joints EZ1 – EZ8, the steel part of the joint below the deck slab is shown. It is obvious from the presented maps of stresses that for the same end-plate configuration and steel parts arrangement, the stress intensities in bare steel joints are more pronounced than those of composite joints. Also it is noticed that for the various reinforcement ratios of the considered reinforced concrete slab, the stress distribution through the joint steel components do not vary significantly. It is visible however, in all presented maps of Huber-von-Mises stresses, that the high stress concentrations are located at the top and the bottom part of the beam and the adjacent parts of the end-plate and the column. On the other hand, the low exertion is placed in the column panel somewhere about the middle of the beam cross-section depth.

Figures 29-32 show the comparison between the deformed shape of end-plates obtained experimentally and numerically. Since the force controlled loading history is applied in experimental investigations, FE load-displacement characteristics extend beyond the ones obtained experimentally. The deformed shape obtained numerically for each conducted comparison is captured therefore at the same joint rotation, equal to that recoded at the ultimate load, and is compared with the end-plate deformation recorded experimentally.

In Fig. 29, the comparison between the actual failure mode of the joint specimens ES1, EZ1 and EZ5 (the flush end-plate joints of 10 mm in thickness) and their deformed shapes from the FE simulation is presented. It is noticeable that the deformation of the end-plate at the ultimate strength is the most intensive in the bare steel specimen ES1 and the amount of deformation decreases when the reinforcement ratio increases.

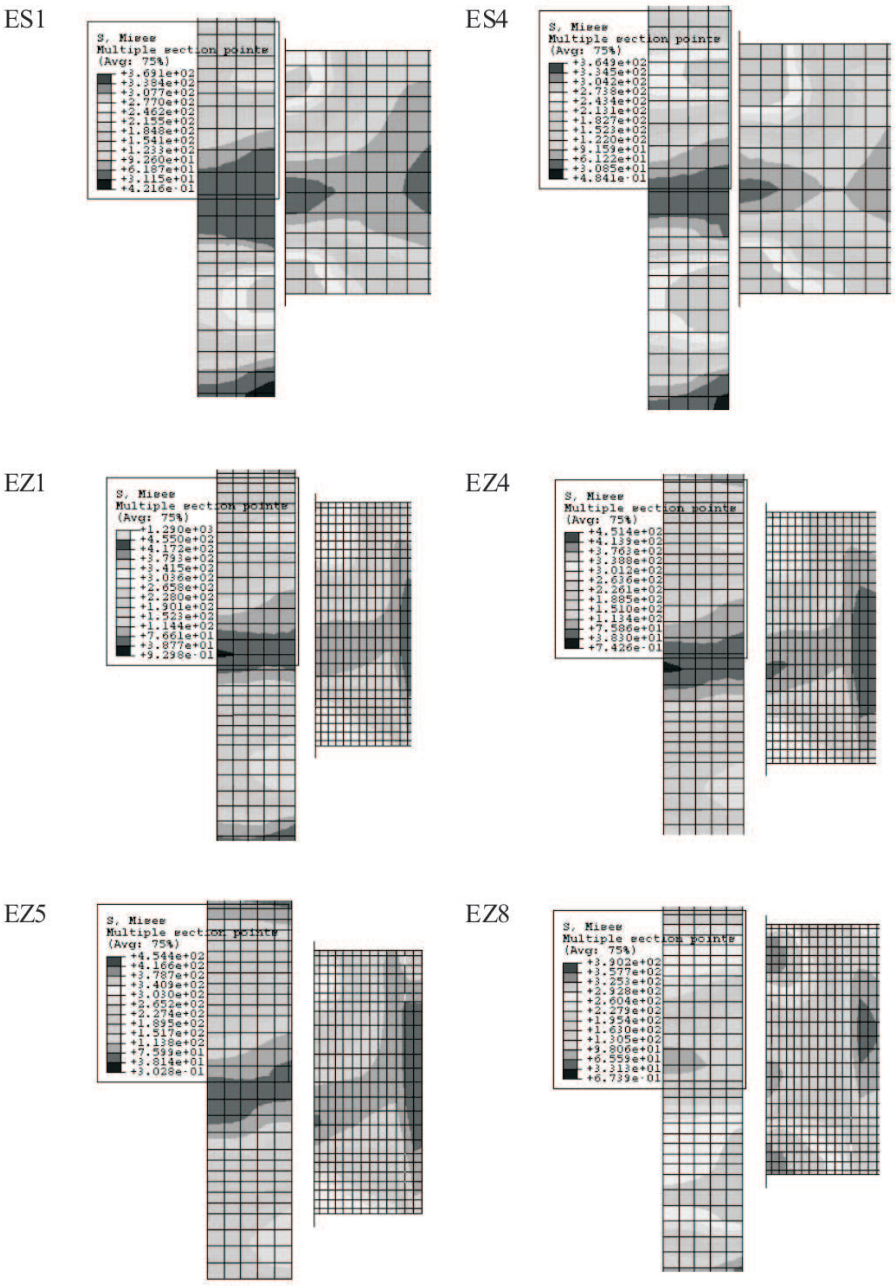

Fig. 27. Huber-von-Mises stress maps for joints with flush end-plates; joint rotation of 30 mrad.
Rys. 27. Mapy naprężeń Hubera-von-Misesa dla węzłów z blachami zlicowanymi; kąt obrotu 30 mrad

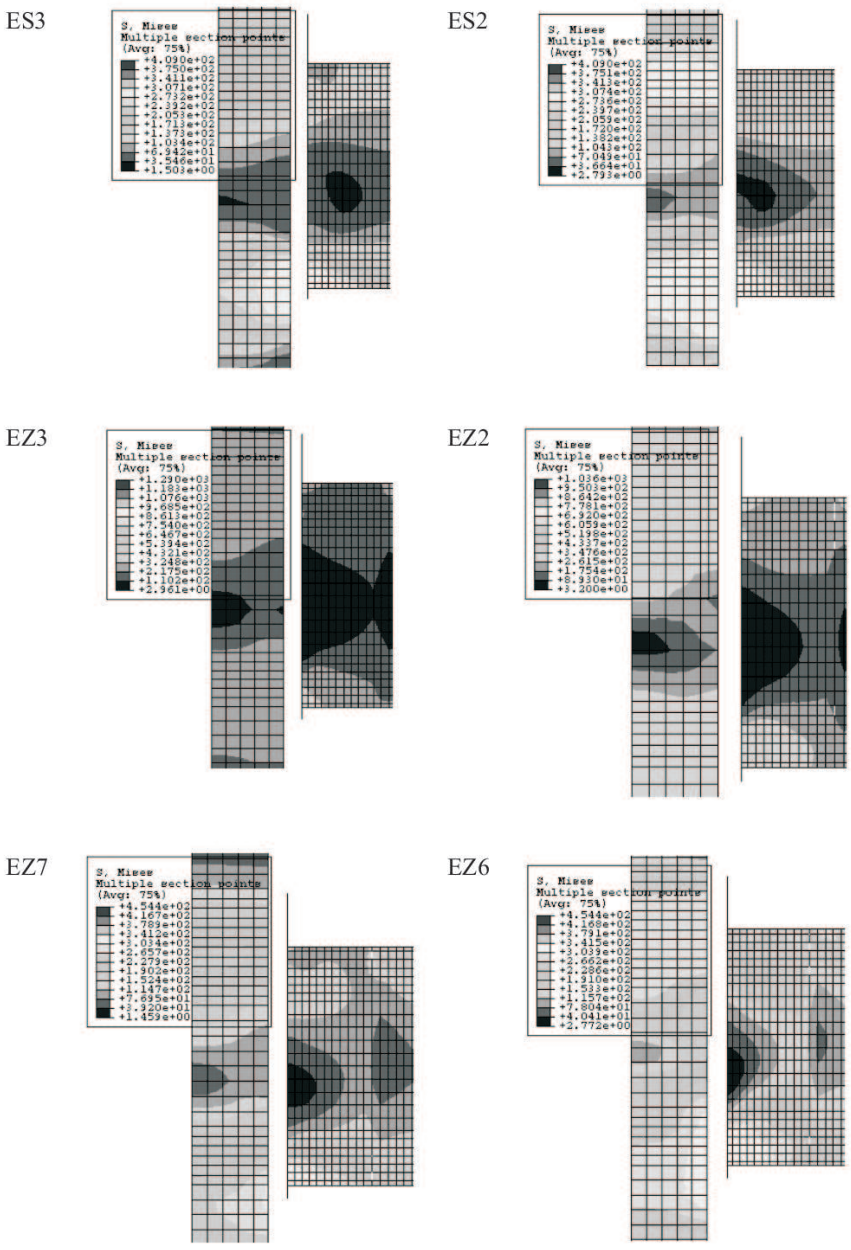

Fig. 28. Huber-von-Mises stress maps for joints with extended end-plates; joint rotation of 30 mrad.
Rys. 28. Mapy naprężeń Hubera-von-Misesa dla węzłów z blachami wystającymi; kąt obrotu 30 mrad

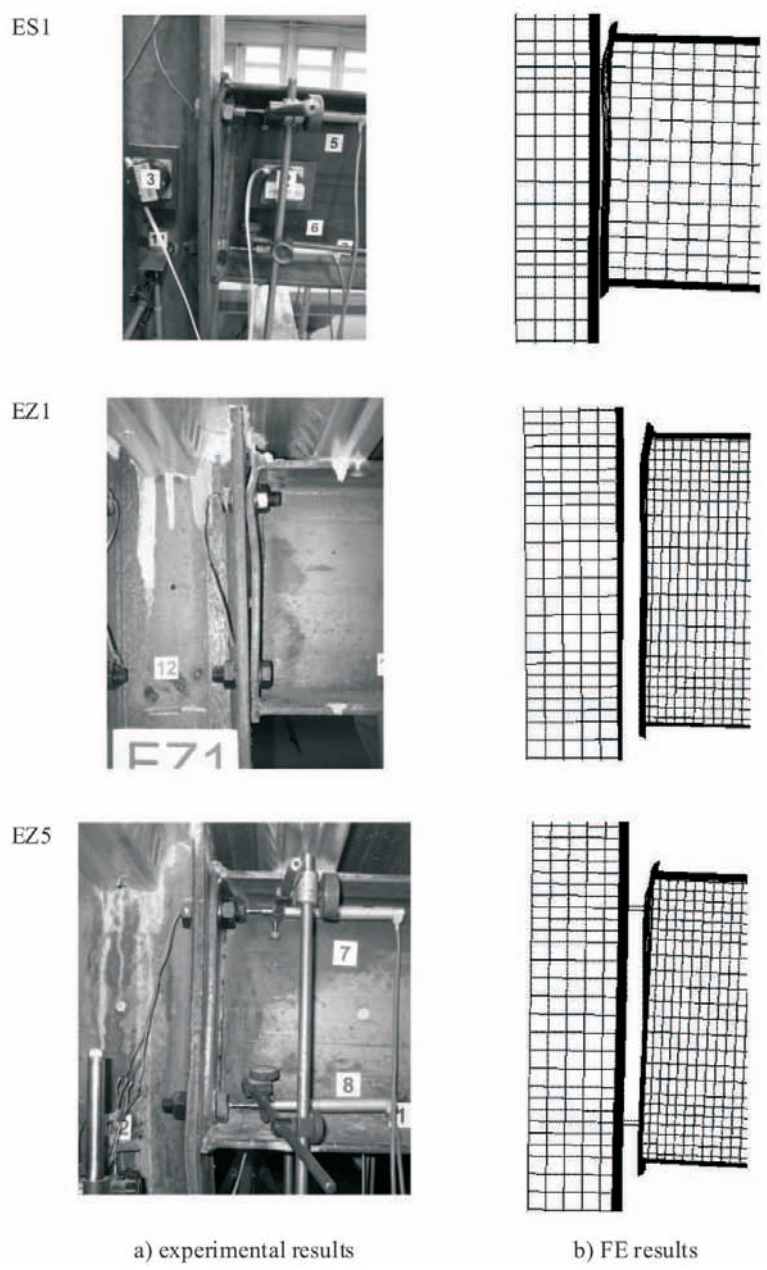

Fig. 29. Deformed shape of joints with 10 mm flush end-plates.
Rys. 29. Odkształcona postać węzłów z blachami czołowymi zlicowanymi o grubości 10 mm

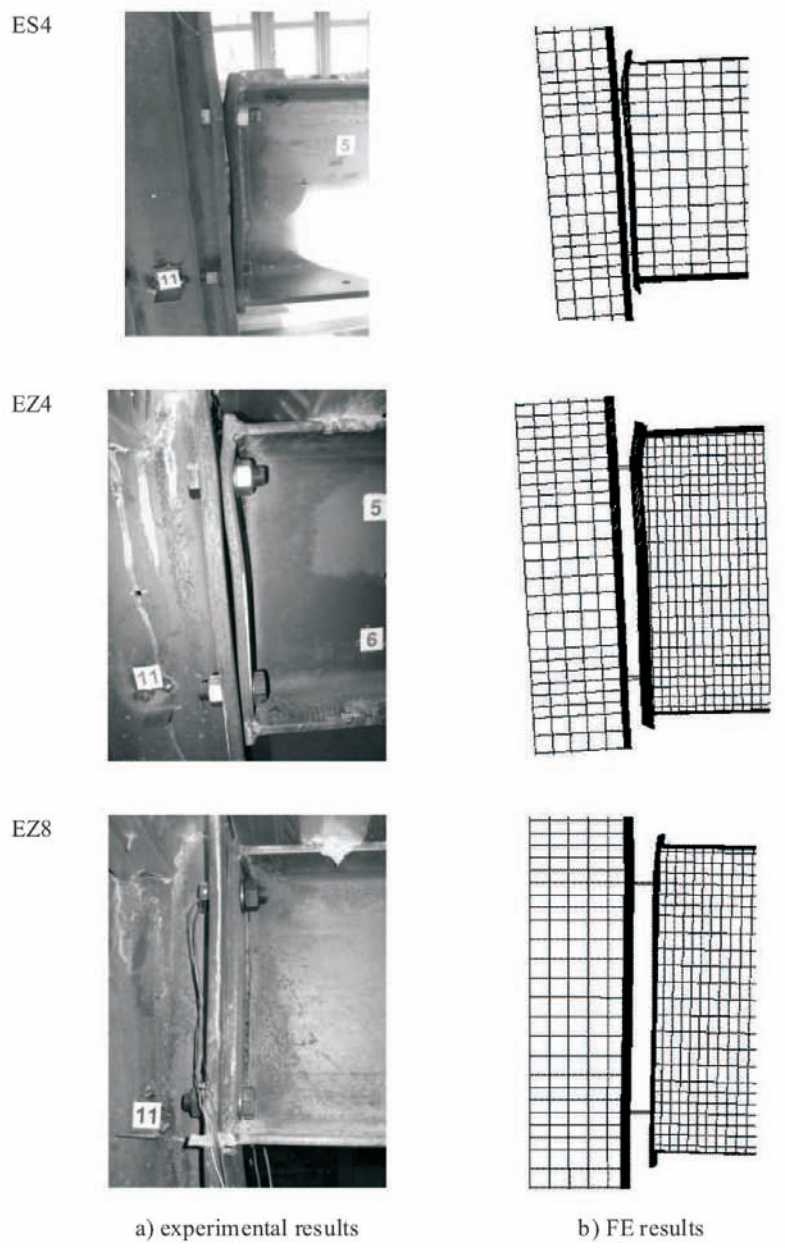

Fig. 30. Deformed shape of joints with 12 mm flush end-plates.
Rys. 30. Odkształcona postać węzłów z blachami czołowymi zlicowanymi o grubości 12 mm

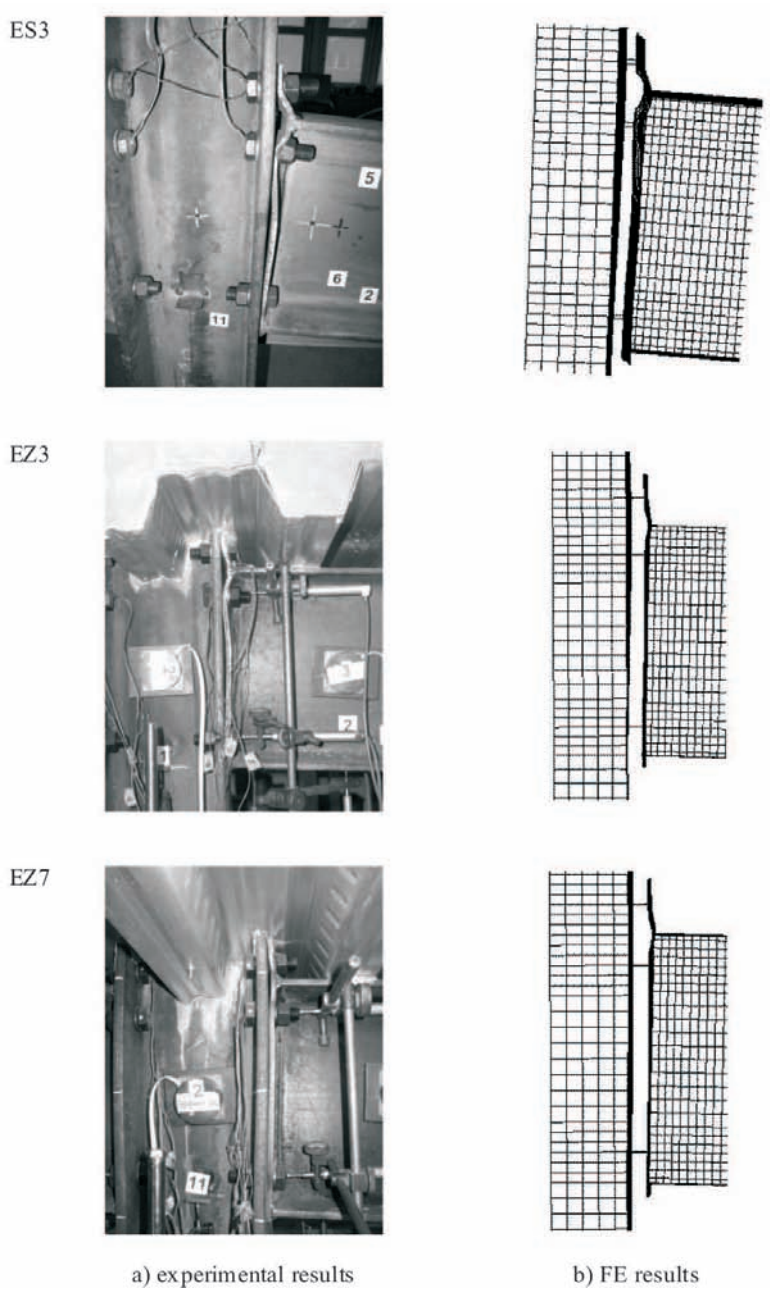

Fig. 31. Deformed shape of joints with 8 mm extended end-plates.
Rys. 31. Odkształcona postać węzłów z blachami czołowymi wystającymi o grubości 8 mm

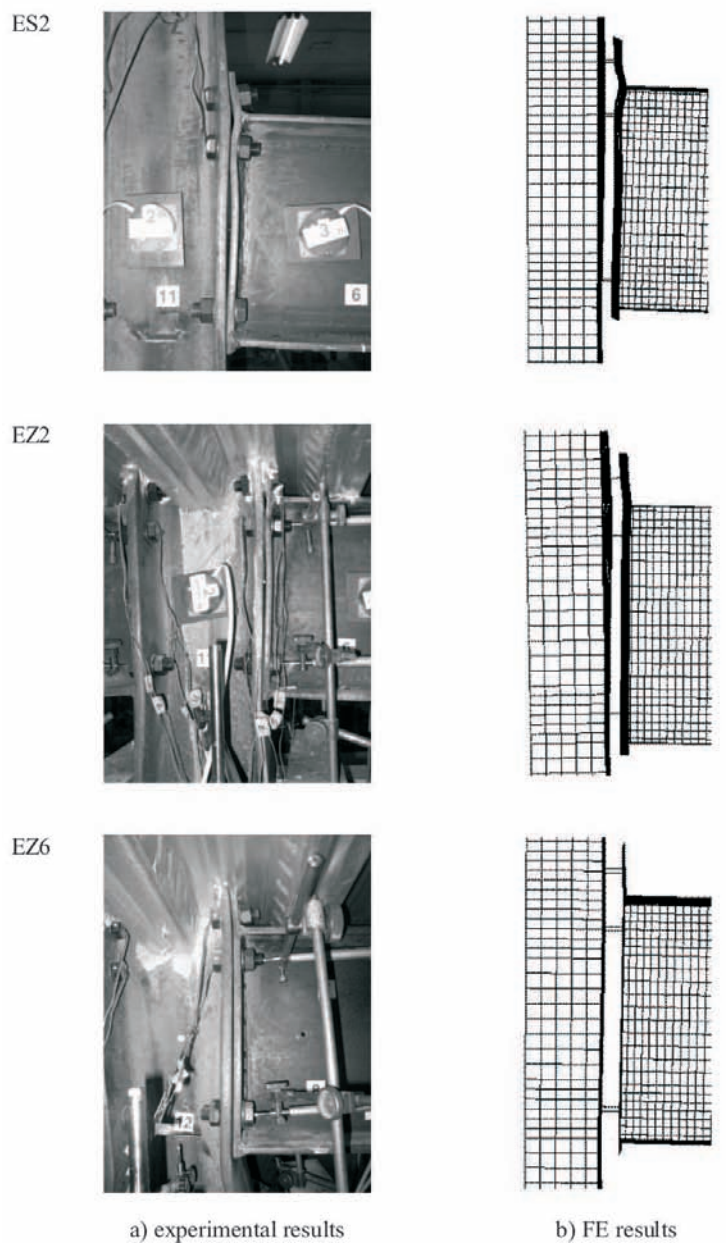

Fig. 32. Deformed shape of joints with 10 mm extended end-plates.
Rys. 32. Odkształcona postać węzłów z blachami czołowymi wystającymi o grubości 10 mm

The shape of flush end-plates is such that the most deformed part is placed above the top bolt row of the joint, i.e. the upper part of the end-plate, in the neighbourhood of its welded connection to the top flange of the beam. The similar observations can be made in case of the comparison presented in Fig. 30 for joints with the flush end-plate of 12 mm in thickness. This figure refers to the specimens ES4, EZ4 and EZ8, and indicates the end-plate deformations similar to those presented in Fig. 29.

For extended end-plates joints, the deformed shapes are depicted in Figs. 31 and 32. For all the joints, a large local deformation appears at the top of the end-plate, above and below the beam top flange subjected to tension. Based on these figures, one can indicate that more ductile behaviour of the extended end-plate joints is achieved for smaller end-plate thicknesses. Also in this case, a lower reinforcement ratio (rebars of 8 mm in diameter) allows for greater end-plate deformability at the ultimate load. For the group of the joints with the reinforcement bars of 12 mm in diameter, the distortion of end-plates is less significant because the failure mode is related in this case to inelastic out-of- plane deformations of the yielded column web panel.

The presented deformed shapes imply a good agreement between the FE and the test results. In all cases, there is lack of substantial elongations of bolts, including those exposed to the highest tensile stresses.

5. Conclusions

Numerical FE simulations are carried out to study the behaviour of composite steel--concrete end-plate joints. A validation exercise is carried out by comparing the results obtained numerically with those recorded in experimental investigations. Comparison is made in terms of the load-displacement characteristics for the point of load application of all the tested joint specimens and the moment-rotation characteristics of these joints. General purpose FE software ABAQUS is used for numerical simulations. The specimen geometric nonlinearity and material inelastic behaviour of all the joint components are considered. Simulation results are compared with experimental data. Obtained FE results show a good agreement between the predicted and measured responses, better in the elastic range and less accurate but seem to be acceptable from the engineering point of view in the inelastic range. This gives a confidence that the FE technique developed is capable of predicting the composite joint responses with an acceptable degree of accuracy from the engineering practice point of view.

An idea of the FE model creation for the considered class of composite joints is based on simply the extension of the modelling technique developed by the authors in [7, 8] for bare steel joints, by adding shear stud elements and the discretized reinforced concrete slab elements modelled with options available in ABAQUS, to the FE model previously developed for bare steel joints. Comparison of the composite joint behaviour with the behaviour of its bare steel counterpart allows, for example, for the evaluation of benefits related to the performance of composite joints with reference to their steel

counterparts with the same configuration and detailing of steelwork. Properly calibrated FE model can be used to further investigate the joint behaviour without a necessity of expensive and time-consuming laboratory tests.

The conducted comparison between the results of the analyzed composite joints implies that the thickness of the end-plate within the range of 40% to 60% of the bolt diameter in composite steel-concrete joints has no significant influence on the joint initial stiffness and only a noticeable influence on the joint ultimate moment is observed. Composite joints with extended end-plates can sustain a higher ultimate moment if compared with those of flush end-plates. Moreover, the joint initial stiffness remains almost the same regardless of the reinforcement ratio. Finally, adding more reinforcement to the concrete slab may lead to a higher moment capacity but to a lower rotation at the ultimate moment.

In an optimally shaped composite joint, it is necessary to ensure a balance between the strength of the joint and the joint deformability. It is expected that for a given joint configuration, there is a possibility of such a joint detailing that the deformation capacities of reinforcing bars and steelwork parts of the joint are accomplished simultaneously. From the conducted experimental tests of composite joints, one can conclude that changing the reinforcement ratio from the low value (for specimens of the first group) to the high value (for specimens of the second group), and keeping the constant values of the other parameters for the same joint detailing, the mode of failure changes from the brittle one (rupture of reinforcing bars) to a ductile one (excessive in-plane plastic deformations of the column web panel in compression followed by its subsequent out-of-plane local instability).

Taking benefits from the ductile behaviour of steel in the end-plate component of steel parts of the composite joint and the reinforcement component of its concrete part, one may prevent the joint from sudden failure, therefore it may allow for the redistribution process of internal forces to take place in the whole structure and to enhance the safety requirements.

In order to achieve a ductile behaviour of the composite end-plate joints, it is necessary to ensure the stress redistribution process to take place among the joint components. Based on the observation from the conducted numerical analysis validated by the performed experimental tests, one can conclude that the use of thinner end-plates and properly balanced ductility through an adequate reinforcement sizing can provide beneficial conditions for inelastic redistribution process to take place. In the application rules proposed in Eurocode 4 [2], it is assumed that when the moment increases the reinforcing bars reach their design resistance before the top row of bolts. In case of ductile rebars possessing reasonable deformation capacity in tension, redistribution of the internal forces can take place and the supplementary bending moments may be applied to the joint in order to be carried by steelwork parts that in turn may subsequently reach their design resistances. From investigations carried out by the authors, the recommendation is to oversize the bolt connectors and allow for the application of thinner end-plates for larger end-plate deformations to appear

before significant stresses may occur in the connectors of the outer bolt rows subjected to tension. Considering the steelwork part of the composite joint and according to the concept of component method introduced in Eurocode 3 [4], the failure mode is ductile, if there is the column web panel failure in yielding due to tension/compression or shear, or the end-plate/column flange yield line mode of failure in bending. It is possible by using thinner end-plates and bolt rows arranged away from the welded connection between the end-plate and the beam section flanges.

The class of end-plate joints considered herein uses end-plates of the thickness being smaller that that used nowadays in practical application and ranging from 40% to 60% of the diameter of bolted end-plate-to-column-flange connectors. The application of such innovative joints in engineering practice may enhance the ductility behaviour of steel frame structures with composite steel-concrete floor systems.

6. Aknowledgements

This paper constitutes a part of the PhD study of the second author and is concerned with the development and validation of the numerical modelling technique used for the evaluation of strength, stiffness and deformability of a certain class of composite steel-concrete beam-to-column joints. The financial support for the PhD study provided by the Ministry of Science and Higher Education in Poland (grant No. N 506 0507 33) is highly appreciated. Numerical work that has been carried out through the Computing Centre of the Warsaw University of Technology is kindly acknowledged.

References

1. L. Simões da Silva, R.D. Simões, P.J.S. Cruz, *Experimental behaviour of end-plate beam-to-column composite joints under monotonical loading*, Engineering Structures, **23**, 11, 1383-1409, 2001.
2. Eurocode 4: EN 1994-1-1: Design of composite steel and concrete structures, Part 1.1: General rules and rules for buildings, CEN, Brussels 2005.
3. J. Bródka, A. Kozłowski, *Stiffness and strength of semi-rigid joints* [in Polish], Oficyna Wydawnicza Politechniki Rzeszowskiej, Białystok-Rzeszów, 1996.
4. Eurocode 3: EN 1993-1-8: Design of steel structures – Part 1-8: Design of joints, CEN, Brussels 2005.
5. A. Kozłowski, *Shaping of the steel and composite skeletal structures with semi-rigid joints* [in Polish], Oficyna Wydawnicza Politechniki Rzeszowskiej, Rzeszów, 2000.
6. J. Bródka, A. Kozłowski, *Steel skeletal buildings* [in Polish], Oficyna Wydawnicza Politechniki Rzeszowskiej, Rzeszów, 2003.
7. M.A. Giżejowski, W. Salah, W. Barcewicz, *Experimental and numerical modelling of steel flush end-plate beam-to-column joints*. [In:] The scientific research problems of building. Monograph publication (Eds. M. Broniewicz, J.A. Prusiel), Wydawnictwo Politechniki Białostockiej, **2**, 225-232, Białystok, 2007.
8. M.A Giżejowski, W. Salah, W. Barcewicz, *Finite element modelling of the behaviour of steel end-plate beam-to-column joints*, Archives of Civil Engineering, LIV, **4**, 693-733, 2008.

9. R.P. JOHNSON, *Composite Structures of Steel and Concrete*. Volume I: Beams, Slabs, Columns and Frames for Buildings, Blackwell Scientific Publications, 1994.
10. B. UY, J.Y.R. LIEW, *Composite Steel-Concrete Structures.* [In:] The Civil Engineering Handbook (Eds. W.F. Chen, J.Y.R. Liew). CRC Press, Boca Raton 2003.
11. W. KUCHARCZUK, S. LABOCHA, *Composite Steel-Concrete Structures of Buildings* [in Polish], Arkady, Warszawa, 2007.
12. V.A. OVEN, I.W. BURGESS, R.J. PLANK, A.A. ABDUL WALI, *An analytical model for the analysis of composite beams with partial interaction*, Computer & Structures, **62**, 3, 493-504, 1997.
13. G. FABBROCINO, G. MANFREDI, E. COSENZA, *Non-linear analysis of composite beams under positive bending*, Computer & Structures, **70**, 77-89, 1999.
14. K. BASKAR, N.E. SHANMUGAM, *Steel-concrete composite plate girders subject to combined shear and bending.* Journal of Constructional Steel Research, **59**, 531-557, 2003.
15. Q.Q. LIANG, B. UY, M.A. BRADFORD, H.R. RONAGH, *Ultimate strength of continuous composite beams in combined bending and shear*, Journal of Constructional Steel Research, **60**, 1109-1128, 2004.
16. K. BASKAR, N.E. SHANMUGAM, V. THEVENDRAN, *Finite-element analysis of steel-concrete composite plate girder*, Journal of Structural Engineering, **128**, 9, 1158-1168, 2002.
17. K.E. BARTH, H. WU, *Efficient nonlinear finite element modelling of slab on steel stringer bridges*, Finite Elements in Analysis and Design, **42**, 1304-1313, 2006.
18. W. CHUNG, E.D. SOTELINO, *Three-dimensional finite element modelling of composite girder bridges*, Engineering Structures, **28**, 63-71, 2006.
19. F.D. QUEIROZ, P.C.G.S. WELLASCO, D.A. NETHERCOT, *Finite element modelling of composite beams with full and partial shear connection*, Journal of Constructional Steel Research, **63**, 505-521, 2007.
20. F. FU, D. LAM, J. YE, *Modelling semi-rigid composite joints with precast hollowcore slabs in hogging moment region*, Journal of Constructional Steel Research, **64**, 1408-1419, 2008.
21. M. GIŻEJOWSKI, W. BARCEWICZ, W. SALAH, *Experimental and numerical modelling of composite steel--concrete flush end-plate beam-to-column joints*. [In:] Research and design issues in construction. Monograph publication (Eds. A. Łapko, M. Broniewicz, J.A. Prusiel) Wydawnictwo Politechniki Białostockiej, Wydawnictwo Politechniki Białostockiej, VI, 41-50, Białystok, 2008.
22. M. GIŻEJOWSKI, W. SALAH, *Solving behavioural issues of composite joints by appropriate finite element modelling*, [In:] Budownictwo i inżynieria środowiska, z. 50, Oficyna Wydawnicza Politechniki Rzeszowskiej, 63-72, 2008.
23. M. GIŻEJOWSKI, A. BARSZCZ, A. KOZŁOWSKI, L. ŚLĘCZKA, *Current practice and future development in modelling, analysis and design of steel semi-continuous frames*. Archives of Civil Engineering, LIV, **1**, 73-128, 2008.
24. ABAQUS/Standard, User's Manual I-III, version 6.6, Hibbit, Karlsson and Sorenson Inc., Providence, RI, 2006.
25. ABAQUS, Theory Manual, version 6.6, Hibbit, Karlsson and Sorenson Inc., Providence, RI, 2006.

SKOŃCZENIE-ELEMENTOWE MODELOWANIE ZACHOWANIA SIĘ PEWNEJ KLASY WĘZŁÓW ZESPOLONYCH STALOWO-BETONOWYCH W POŁĄCZENIACH RYGLI ZE SŁUPAMI

Streszczenie

Węzły w konstrukcjach ramowych można sklasyfikować jako sztywne (o pełnej nośności), podatne (o niepełnej nośności) lub nominalnie przegubowe, w zależności od ich typu, konfiguracji i rozmieszcze-

nia łączników. Węzły o pełnej nośności są wymagane dla ram sztywnych, w których założono, że węzły zapewniają pełne przeniesienie momentów zginających z rygli na słupy. Natomiast w ramach z węzłami podatnymi o niepełnej nośności, węzły są charakteryzowane przez względne obroty pojawiające się pomiędzy łączonymi elementami tak, że moment zginający może być przeniesiony tylko częściowo. W ostatnich latach, idea wykorzystania bezżebrowych węzłów podatnych zyskuje coraz większe zastosowanie w praktyce inżynierskiej. Ramy niepełnociągłe mogą przeciwstawiać się oddziaływaniom dzięki węzłom podatnym o niepełnej nośności, które przenoszą momenty zginające przy jednoczesnym pojawieniu się lokalnego obrotu elementów przerwanych w węźle. Jednym z efektywnych sposobów zwiększających ciągliwość węzłów typu rygiel – słup z blachami czołowymi jest zastosowanie blach o grubości mniejszej niż stosowana obecnie w praktyce inżynierskiej. W niniejszej pracy, poddano analizie grupę węzłów zespolonych stalowo-betonowych, w których grubość blachy czołowej stanowi około 40-60% średnicy śrub. Praca stanowi rozwinięcie zagadnień opracowanych przez autorów w powoływanych pracach wcześniejszych i dotyczących numerycznego modelowania zachowania się węzłów stalowych w konstrukcjach ramowych.

Celem rozważań jest znalezienie prostego i jednocześnie wystarczająco dokładnego modelu 3D zachowania się węzła zespolonego, uwzględniającego najistotniejsze czynniki wpływające na zachowanie się stalowo-betonowych węzłów doczołowych z blachami o grubościach mniejszych niż stosowane w rozwiązaniach konwencjonalnych. Przedstawiono model 3D skonstruowany dla rozważanego typu węzłów zespolonych, przy wykorzystaniu systemu ABAQUS oraz porównano wyniki symulacji numerycznych z wynikami badań doświadczalnych przeprowadzonych w Politechnice Warszawskiej. Porównanie wyników nieliniowego modelu skończenie – elementowego z wynikami badań doświadczalnych węzłów zespolonych w skali technicznej, świadczy o poprawności przyjętej techniki modelowania, jak również o zadowalającej zgodności modelu numerycznego z modelem fizycznym elementów badanych doświadczalnie. Na zakończenie podano praktyczne uwagi dotyczące innowacyjnego kształtowania i projektowania rozpatrywanej klasy węzłów zespolonych.

Remarks on the paper should be sent to the Editorial Office no later than June 30, 2010

Received December 01, 2009 revised version March 15, 2010